Potential impact of climate change to the future climate and streamflow of the Mackenzie River Basin

by

Lia Pervin

A thesis submitted in partial fulfillment of the requirements for the degree of

Master of Science

in

Water Resources Engineering

Department of Civil and Environmental Engineering

University of Alberta

Abstract

The Mackenzie River provides a critical corridor for Canada's Arctic transportation network and the Mackenzie River Basin (MRB), the largest river basin of Canada, has been subjected to the impact of climate change. In this study, we have investigated the potential impacts of climate change on the MRB that could significantly alter the hydrology of the river basin. A regional climate model called WRF (Weather Research and Forecasting model) was set-up and fine-tuned to simulate the possible impact of climate change to MRB. WRF was sensitive with respect to parameters of the land surface scheme and micro physics options. Through a detailed fine tuning (calibration) process, by setting up WRF with the Noah Land Surface model, the Double Moment 6–class microphysics schemes, the CAM Shortwave and Longwave schemes, we found that WRF could generally simulate realistic climate over the MRB. The one-degree resolution, ERA-Interim data were used as input to WRF to simulate the regional climate of MRB which were validated against gridded observed climate data ANUSPLN of Environment Canada. The temperature and rainfall data that WRF dynamically downscaled from the ERA-Interim data as input generally compares well with the ANUSPLIN data, as well as some station climate data during the validation period (1979 to 1991). Next, using this model setup, future climate of MRB were simulated to assess the regional impact of climate change over the MRB. We used the CanESM2 global climate model (GCM) outputs at 275 km by 275 km (resolution) as the initial and boundary conditions to WRF model for simulating the climate of MRB for the base (1979 to 2005) as well as the future periods based on the CanESM2 RCP 4.5 and RCP 8.5 climate change scenarios over 2050s (2041 to 2070). The regional climate of MRB was simulated at 30 km x 30 km resolution every 6 hour for May, June, July, August, September and October (MJJASO) for each year. Comparing with the base period, the RCP 4.5 climate scenarios generally project a 2

to 4 ° C warming over MRB, particularly over the North and Western side of MRB, while the rainfall is projected to increase by about 75 mm for MJJASO over the MRB by 2050s. As expected, under RCP 8.5 climate scenarios, more pronounced warming is projected than RCP 4.5, with a 2 to 5^{o} C rise in temperature in 2050s and the rainfall is projected to increase by about 85 mm over MJJASO and the spatial coverage of changes are projected to be larger than that of RCP 4.5 rainfall. Therefore, wetter and warmer climate are expected by 2050s from the WRF simulation for both RCP 4.5 and RCP 8.5 scenarios. Under the projected increase in air temperature and precipitation of RCP 4.5 climate change scenarios of the CanESM2 GCM of IPCC (2013) downscaled by WRF, the streamflow of the Mackenzie at the Fort Simpson and Arctic Red River stations are simulated using the conceptual hydrologic model HBV of Sweden. The streamflow for is projected to decrease mainly because more evaporation loss projected under a warmer climate is expected to offset the projected increase in summer precipitation over the MRB in 2050s. The projected decreased streamflow in could significantly affect the water resources and thus the navigability or northern transportation of the Mackenzie River in future.

Preface

This thesis is an original work by Lia Pervin. No part of this thesis has been previously published

Acknowledgements

I would like to express my deepest gratitude to my supervisor, Dr. Thian Y Gan, for being a great source of expertise throughout this study and for his invaluable support and encouragement. This thesis could not have been completed without his help and contributions. Thank you for believing I could succeed and for giving me the opportunities to do so.

My gratitude and appreciation also extends to my parents for their continual support and endless love. I owe my deepest gratitude to them for fostering in me the desire to learn and the motivation to succeed.

Finally, I would like to express sincere thanks to all my friends and colleagues in the Water Resources Engineering of the Department of Civil and Environmental Engineering at the University of Alberta who have encouraged me by sharing ideas.

This study was funded by Transport Canada under the Northern Transport Adaptation Initiative (NTAI) program. The ANUSPLIN, HYDAT, climate station data, NARR data, PCIC statistically downscaled RCP climate scenarios, GCM climate scenarios data of CMIP5 and ERA-Interim reanalysis data, etc., were downloaded from the websites of Environment Canada NCEP, PCIC of University of Victoria, ESGF and ECMWF, respectively. Supercomputing resources of this study was provided by Compute Canada's WestGrid supercomputing program. The regional climate model, WRF (Weather Research and Forecasting), was downloaded from the website of wrf-model.org, while the hydrologic model, HBV, was provided by Dr. Seibert of University of Zurich, Switzerland.

Table of Contents

List of Figures

List of Tables

List of Abbreviations

ACM2	Asymmetric Convection Model 2
ARW	Advanced Research WRF
CCCma	Canadian Centre for Climate Modelling and Analysis
CanESM2	The 2nd generation Canadian Earth System Model
ERA-Interim	A global atmospheric reanalysis from 1979, continuously updated in real time
ET	Evapotranspiration
ECMWF	European Centre for Medium-Range Weather Forecasts
GCMs	General Circulation Models
GPCP	Global Precipitation Climatology Project
IPCC	The Intergovernmental Panel on Climate Change
LAI	Leaf area index
LSM	Land surface model
MRB	Mackenzie River Basin
MSLP	Mean sea level pressure
NARR	North American Regional Reanalysis
NCEP	National Centers for Environmental Prediction
NCAR	The National Center for Atmospheric Research
NWP	Numerical Weather Prediction
RRTM	Rapid Radiative Transfer Model
RCP	Representative Concentration Pathways
RUC LSM	Rapid Update Cycle Land Surface Model
WRF	The Weather Research and Forecasting (WRF) Model
WPS	WRF Preprocessing System

CHAPTER ONE

INTRODUCTION

1.1 Introduction

Over the last century the world has become more and more industrialized, where most countries focus on economic growth and industrialization. As a result, man is putting pressure on the mother earth by emitting greenhouse gases, which have led to global warming problems observed in recent decades. According to the IPCC 5th assessment report that "It is extremely likely that human influence has been the dominant cause of observed warming since mid-20th century", for human activities have affected the Earth's energy budget by increasing the atmospheric concentrations of greenhouse gases such as CO_2, methane, nitrous oxide, and aerosols and by changing land surface covers.

Instrumental records years show that land and sea surface temperatures have been increasing over the last or more 100 years (IPCC 2013). Different observations, made by different groups in various countries using different technologies, show the strong sign of the climate change on our globe. More and more powerful numerical weather prediction models have been developed in recent years which can model the historical climate of the mother Earth reasonably well, and therefore are useful to project future long term climate. Results of climate model simulations provide evidence on how the earth's climate has been changing since the mid- 1950s. The long term increase in air temperature globally has modified the energy and water fluxes, and thus the hydrological cycle; some parts of the world have experienced heavy rainfall and floods while others suffer from droughts, since the distribution of atmospheric water vapor varies spatially

across the world. Rising air temperature may accelerate the atmospheric moisture transport which could alter the climate system (Newton et al. 2014). It seems that globally extreme weather events have changed in terms of their extensiveness, severity and the frequency of occurrences (Bowden et al. 2013). According to climate model projections, in coming decades the world will continue to experience warmer temperature than the past, which will continue to affect the climate and hydrologic patterns on earth (IPCC 2013). To understand possible climate change impact at regional scale, it is essential to use a regional climate model at much higher resolutions than that of General Circulation Models (GCMs) which can only simulate future climate at a resolution of 250-400 km which is too coarse to capture regional climatic processes accurately. As any other country, Canada is expected to experience impact of climate change which could affect our water resources, and subject us to effects of hydrologic extremes such as floods and droughts.

Global warming, primarily due to the radiative forcing of increasing greenhouse gases such as CO_2, is expected to result in more atmospheric water vapor pressure because at typical lower troposphere temperatures, the saturation vapor pressure will increase by about 7% for every 1°K rise in temperature according to the Clausius-Clapeyron relationship (Held and Soden 2006). Therefore we expect rising atmospheric temperature will affect the precipitation pattern especially in higher latitudes where more pronounced warming has been projected. Therefore changes in the hydrologic cycle would occur as temperature increases, and observations along these lines have already been documented (Kunel et al. 1999; Groisman et al. 2004; Pryor et al. 2009).

From analyzing trends in Canadian temperature and precipitation during the 20th century, Zhang et al. (2000) concluded that from 1900 to1998, the annual mean temperature has increased

between 0.5 and 1.58C in the south, whereas more intense warming occurred in the west, commonly during spring and summer periods. In the meantime the Southern part of Canada got to be about 5% to 35% wetter. It seems that climate has become gradually wetter and warmer in southern Canada throughout the entire century.

Changes to seasonal air temperature and precipitation can have significant long-term impact to the hydrology of river basins across the world, including that of Canada, where the Mackenzie River Basin is the largest river basin of about 1.8 million km^2 in area. Being the largest river basin in Canada that extends from central Alberta to the Arctic, the Mackenzie River Basin is expected to subject to significant impact of climate change. Several studies has pointed out that the Mackenzie River Basin is experiencing some of the greatest rise in temperature anywhere in the world (Wayland 2004) and the studies also have concluded that over the last few decades the warming trend is going up sharply in Canada including the MRB (Wayland 2004; Shabbar et al. 1997; Zhang et al. 2000; Aziz 2006). Conversely, we expect climatic change will modify the future water resources of MRB, especially during summer when there will be more demand for water to adequately maintain aquatic and terrestrial ecosystems (Trenberth et al. 2007; Stewart et al. 2004), agricultural production, northern ferry operations and hydroelectricity generation.

Based on the Representative Concentration Pathways (RCP) climate change scenarios of IPCC (2013), how will climate change affect the streamflow of MRB in future? This question has not been well addressed based on the simulations of any high resolution regional climate model. Therefore the key objective of this study is to address the possible impact of climate change on the streamflow and water levels of the Mackenzie River based on the simulations of a RCM

driven by boundary conditions of some selected Global Climate Models (GCM). The outcome of this study will provide with some quantitative estimate of possible hydrologic changes over the MRB in the future. The results could be utilized by government and non-government organizations, such as the Government of the Northwest Territories, and the Northern Transportation Company Ltd. which operates ferries for the northern transportation network.

1.2 Research Objectives

What could be the impact of climate change to the hydrology of a large-scale river basin located across western Canada? The objectives of this project are as follows:

- To use a regional climate model (WRF) to dynamically downscale the coarse resolution (2.81^{o} x 2.81^{o}) climate change scenarios of a general circulation model (GCM) of IPCC (Intergovernmental Panel of Climate change) to a finer, 30 km x 30 km, resolution appropriate to model the hydrology of the Mackenzie River Basin (MRB).

- To analyze the projected change in temperature and precipitation of MRB in the 2050s based on the downscaled climate change scenarios of WRF.

- By forcing a conceptual rainfall runoff model, HBV, with the downscaled climate change scenarios of WRF, investigate the impact of climate change to the streamflow of MRB in the 2050s.

1.3 Organization of the thesis

A general introduction to climate change impact to river basins has been described in Chapter one, together with objectives of the study. The study site, MRB, its present and past climate, and trends in climate change and literature review are elaborated in Chapter 2; the research

methodology, future climate scenarios (RCP), and datasets of this study are given in Chapter 3; the selection of a mesoscale or regional climate model for assessing the impacts of climate change, the fine tuning of this model and pre-processing of input data and model output, the setting up, calibration and validation of the conceptual hydrologic model, HBV, etc., are described in Chapter 4; and summary and conclusions are given in Chapter 5.

CHAPTER TWO

CLIMATE AND HYDROLOGY OF MACKENZIE RIVER BASIN

2.1 Study Area

Mackenzie River Basin (MRB), a high latitude, regional river basin with a total area of about 1.8 million square kilometers, extending from 52˚ to 69˚ N and 140˚ W to 102˚W, is the largest river basin in Canada. MRB can be sub-divided into seven major sub-basins, which are the Athabasca (upper and lower), the Peace, the Liard, the Peel, the Great Slave, and the Mackenzie-Great Bear river basin (Figure 1). On the other hand, the river basin can also be described with three major physiographic regions: the Cordillera, the Interior Planes and the Precambrian Canadian Shield. MRB possesses an unique hydrological and environmental characteristics with continuous permafrost at the north and sporadic permafrost at the south. The atmospheric circulation in MRB is greatly influenced by its topography. The Rockies at the west and the lower altitude at the center induce strong atmospheric circulations; the three major lakes and wetlands in the north also affect the energy and water fluxes of MRB (Woo et al. 2008).

The Mackenzie River discharges into the Arctic Ocean at an annual average discharge of 9,910 cubic meters per second and hence contributes a significant amount of freshwater to the world's oceans (Wayland 2004). Further, the Mackenzie River plays a key role to the transportation of northern communities of NWT, e.g., the Mackenzie River represents a critical corridor in Canada's Arctic transportation network. In terms of ground transportation, ice roads provide the essential transportation across MRB in the winter (Prolog Canada 2011).

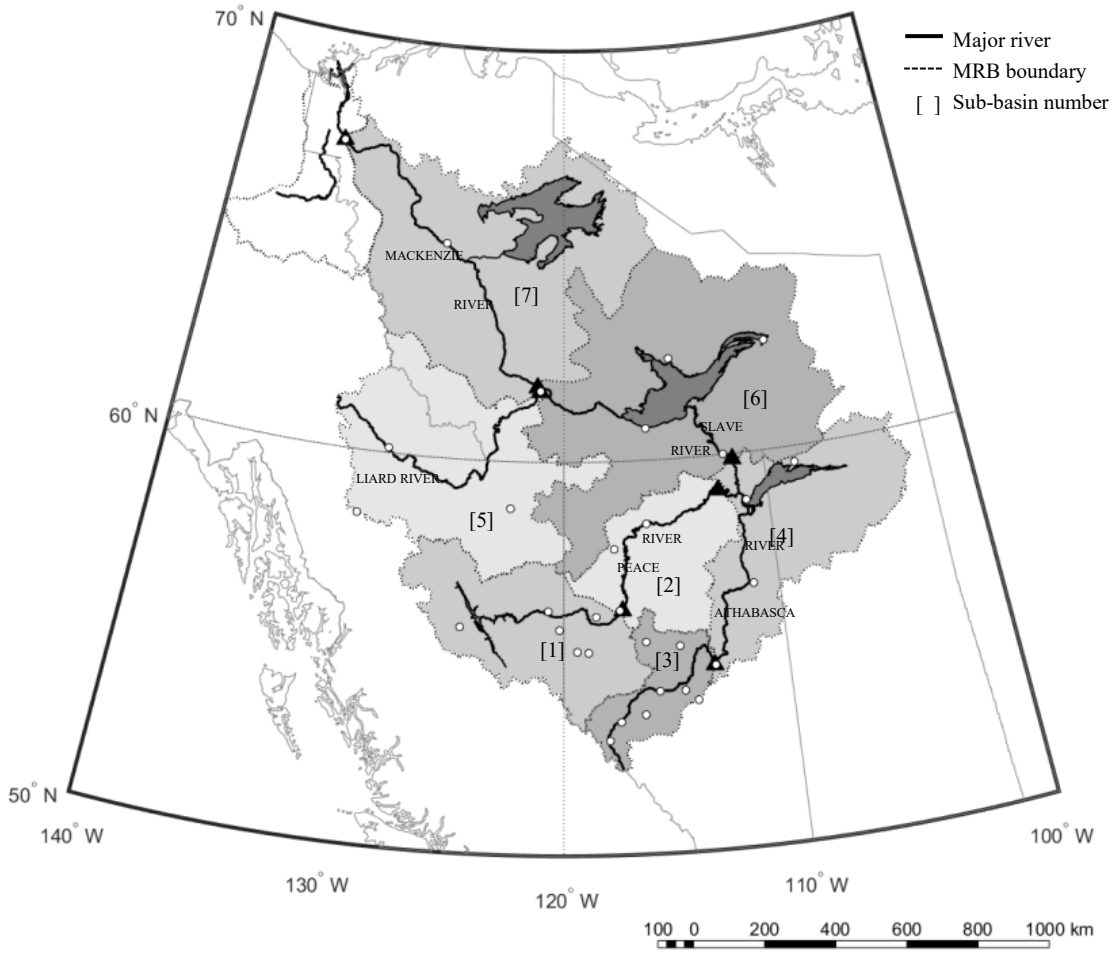

Figure 1: The Mackenzie River Basin of Canada with seven sub-basins.

During the relatively short open water season, the Mackenzie River carries barge traffic for community resupply, including bulk fuel shipments (Prolog Canada 2011; Arctic Theme Page 2009). The Mackenzie River is also a highly active transportation corridor for residents. Most people living along the river travel by snowmobile on the ice cover in winter, and by personal watercraft in the summer. In other words, the water levels of the Mackenzie River play a major role to the transportation of the northern communities of NWT in the summer.

2.2 Topography and Climate of MRB

The western part of MRB is mountainous (Mackenzie and Rocky Mountains), has an average elevation about 1000 m, whereas the interior part is a plain and the eastern part is the Canadian Shield. Continuous frozen ground or permafrost is found in the north because of harsh winter, while forests dominate the southern parts of the basin. The basin has a diversified land cover including farmlands in the southern lowlands and the Peace River basin. Forest covers a large part of the basin, the boreal forest, deciduous forest, coniferous forest and the tundra. Figure 2 shows the Land Cover Class map of MRB. Figure 3 shows the terrain characteristics of the basin.

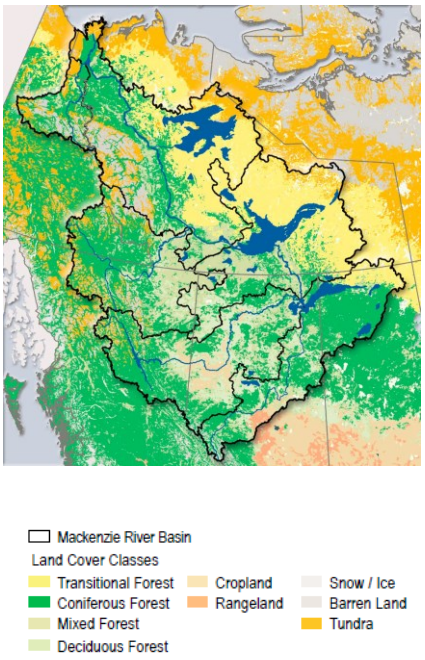

Figure 2: MRB Land use map
(Source: Agriculture and Agri-Food Canada 2015)

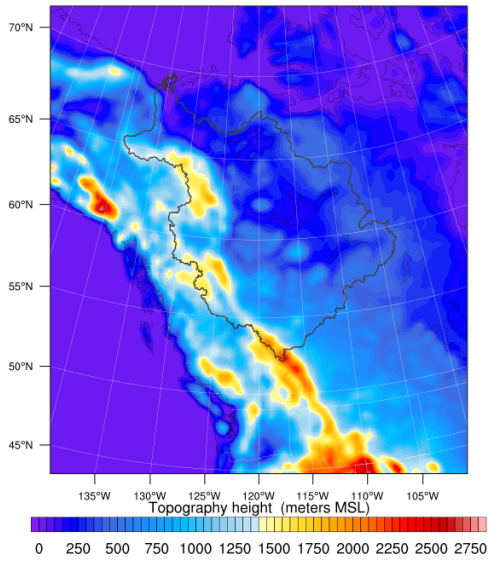

Figure 3: Terrain characteristics of MRB

The northern part of the basin experiences harsh winter, with subzero temperature for the whole winter, with an average winter temperature ranging from -25°C to -35°C, and -50°C is not uncommon; whereas in the summer the average monthly temperature ranges from 8°C in the

north to 20 ^{o}C in the south, which could be as high as 35^{o}C. So the inter-annual temperature variation is fairly substantial within this region. From 1979 to 1998 the average annual precipitation over the MRB was about 410mm, where the July rainfall was above 60 mm (Szeto et al. 2008a), e.g., that a large part of the annual precipitation occurs during summer. Even though large scale atmospheric forcing is generally weak in the summer, MRB could receive moisture from southern Plains and the Atlantic Ocean (Brimelow and Reuter 2008).

The long hour daily solar heating at the summer causes active moist convection. The external moisture fluxes receive through its southern boundary, interacts with the local evaporation to produce summer precipitation. Szeto et al. (2008b) reported that the moisture recycling and the land-air interaction plays a significant role in the summer precipitation over MRB. The low pressure system over the MRB can contribute to the development of extreme precipitation events at summer; whereas the large scale high pressure system could suppress the mountain plane circulation (Brimelow and Reuter 2005). The summer atmospheric features are of particular significance, since it contributes a lot to the water and energy budget of the MRB as well as to the hydrology of the basin. Therefore the surface runoff and the river discharge are greatly affected by the summer temperature and precipitation.

2.2.1 Temperature

Over the past century the global average air temperature has increased by about a degree Celcius (IPCC 2013). Recent studies of climate trends indicate that the global mean annual surface air temperature is increasing at higher rate than before (GISTEMP Team 2015). Frost-free seasons and the growing season in many regions of the Northern Hemisphere have become longer due to global warming, which is also consistent with a long-term significant decrease in the spring snow

cover over Eurasia. Considerable spatial and temporal variations of climatic variables have occurred during the last century, and warming and increasing precipitation trends vary widely across the world.

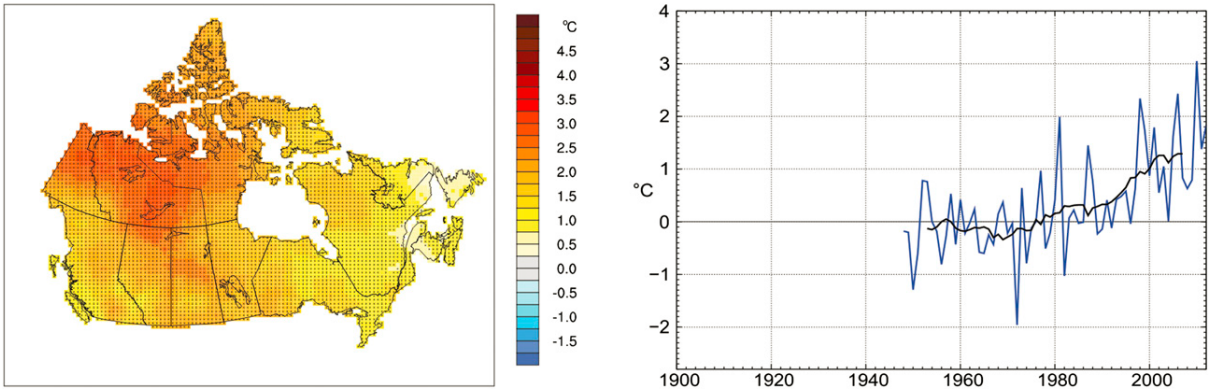

Figure 4: (a) Annual mean temperature anomalies of Canada from 1961-1990 and (b) Trends in the annual mean temperature of Canada for 1948–2012. (Source: Vincent et al. 2015)

The northern region was reported as the most rapid warming region on Earth (Alexander et al. 2006). This warming has been accompanied by significant changes in many other climate elements, including increases in precipitation (Mekis and Vincent 2011), but decrease in annual snow cover duration and streamflow. On an average, Canada has warmed by more than 1.3°C since 1948, a rate of warming that is about twice the global average (Natural Resources Canada 2016). Vincent et al. (2012) found significant increasing trends in the annual mean temperature, with a warming of 1° C to 3° C across Canada over 1948–2012. Figure 4 (a) shows mean temperature departures from 1961 to 1990 normal and linear trend for Canada and climatic regions 1948 to 2012 are shown in Figure 4 (b) the black line is an 11-yr running mean. It was also reported that the seasonal mean air temperature anomalies (averaged over Canada) increased by 1.48 °C [0.88–1.88C] over 1948–2012 during the summer.

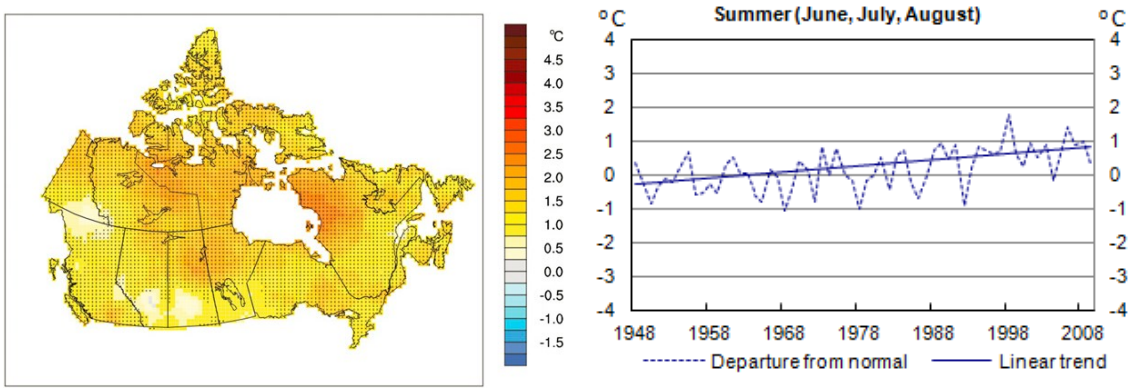

Figure 5 : (a) Trends in the mean temperature for 1948–2012 for summer (adapted from Vincent et al. 2015) (b) Summer mean temperature trend for Canada, 1948 to 2009 (source: Statistics Canada 2015)

The summer air temperature has shown consistent positive trends all over Canada. Figure 5 (a) and (b) show the mean summer temperature trend for Canada. Analyses of daily temperature extremes indicate trends consistent with warming, fewer cold nights, cold days, and frost days, but more frequent warm nights and warm days (Vincent and Mekis 2006). The observed warming trends and global climate model's simulations likely demonstrate the influence of anthropogenic greenhouse gases in Canada (Zhang et al. 2000).

2.2.2 Precipitation

A number of studies have documented the changes in precipitation; most of the world has tended towards wetter conditions during the 20th century (Alexander et al. 2006). Global precipitation over land has increased about 1%; however, occurrence of intense precipitation is reported as more frequent in many mid-to-high latitude regions. There has been a global decrease in the number of consecutive dry days, and an increase in the number of wet days (Kiktev et al. 2003). Frich et al. (2002) have also reported an increase in the frequency of heavy precipitation events

in many areas of the world. They also documented an increase in the maximum 5 day precipitation totals over much of the globe (an indication of more flood-producing events); though changes in precipitation are less spatially coherent than the changes in global air temperature.

Representative trends in precipitation are more difficult to estimate, primarily because of a wide range of spatial and temporal variability of precipitation. However it could be estimated that on an average Canada had become wetter during the past half century, by about 12 % (Environment Canada, 2003). Figure 6 illustrates linear annual precipitation trends (% change) observed across Canada between 1948 and 2012, which shows that almost 45 percent of positive changes in precipitation happened in Northern parts of Canada. Increasing trends in precipitation has been attributed to increase in extreme daily precipitation amounts during the growing season (Qian et al. 2010).

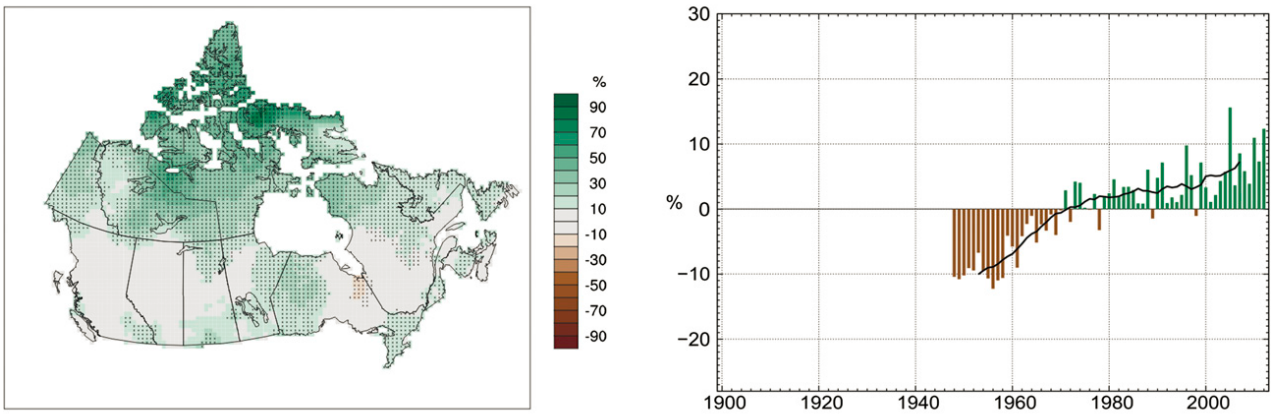

Figure 6: (a) Trends (%) in the annual total precipitation of Canada for 1948–2012 (b) Annual total precipitation anomalies in percentage for Canada (1948–2012). The black line is an 11-yr running mean (Adapted from Vincent et al. 2015).

Observed changes have been generally consistent with a warming climate. An increase in global mean temperature would be followed by an increase in the saturation vapor pressure and, thus an

increase in the overall content of water vapor in the atmosphere (Trenberth et al. 2003). The latter has been observed over most of the Northern Hemisphere. The spatial average of anomalies (averaged over the country) indicates a significant increase of 19% (15%–22%) during the past 65 yr (Vincent et al. 2015). Summer precipitation has mostly increased over Canada in the last four decades. However, some regions are experiencing a minor declining trend, as shown in Figure 7 for 1948–2012.

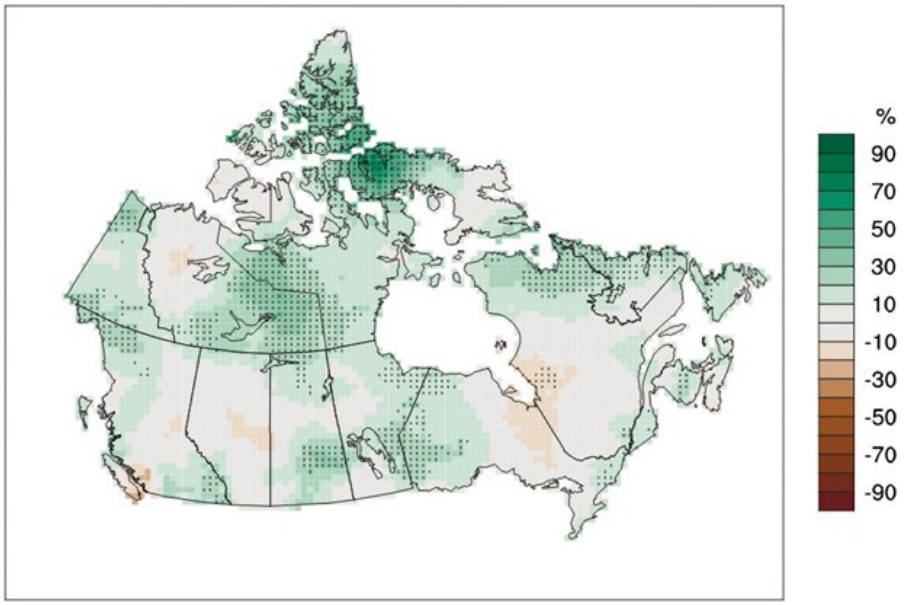

Figure 7: Trends in the total precipitation of Canada for the summer (MJJA) 1948–2012.

2.2.3 Streamflow of the Mackenzie River

The daily discharge of Mackenzie River at the downstream station of Arctic Red usually varies between 15,800 m^3/s and 35,000 m^3/s, lowest and highest respectively. For May to October, daily peak flows occur in the spring to early summer due to snowmelt and breakup of river ice and summer flows are also high. It was observed that the peak flow occurred mostly in May or in June. Trend analyses reveal a statistically significant (85% confident) tendency of decreasing

peak flow by about 3000 m^3/s over 1973-2011 as shown in Figure 8 and Figure 9 (Yang et al. 2015).

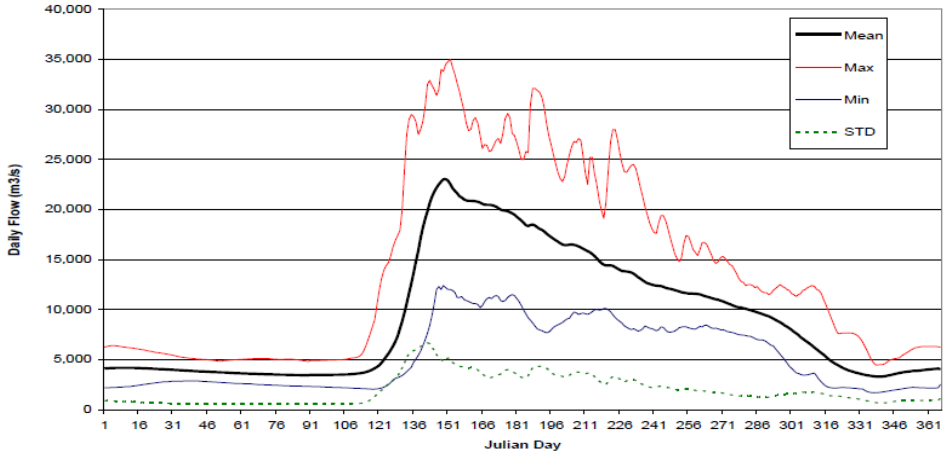

Figure 8: Daily max, min, mean, and standard deviation of the streamflow of Mackenzie at the Arctic Red station in 1973-2011 (adapted from Yang et al. 2015)

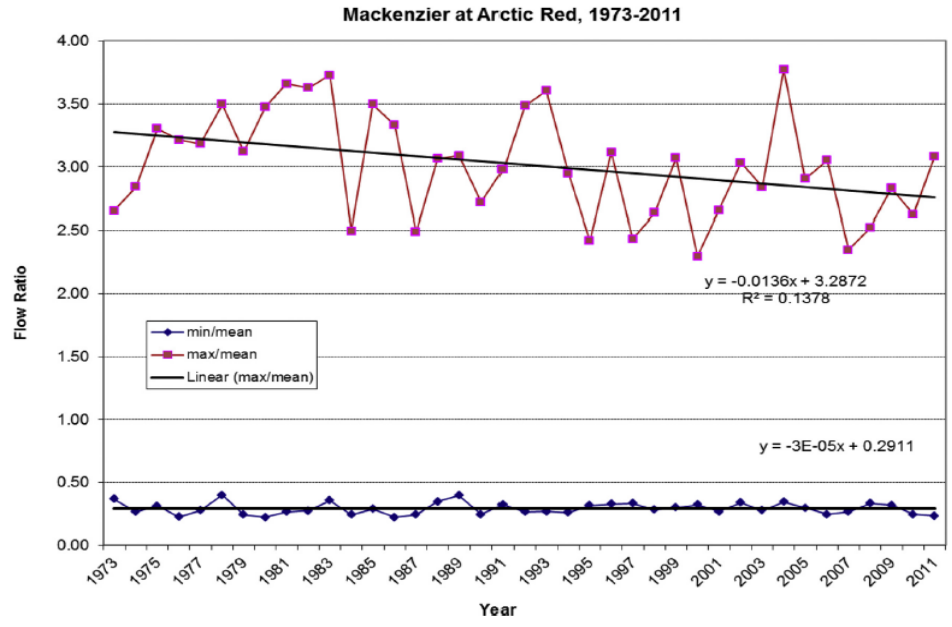

Figure 9: Time series and trends of ratios of daily max/daily mean flows, and daily min/daily mean flows, 1973-2011(adapted from Yang et al. 2015)

2.3 Long-term Climate and Hydrologic Projections of MRB

In a warmer climate, global climate models projected an increase in the mean precipitation (IPCC 2013), although the different parts of the world will experience different changes. The whole of Canada, with the possible exception of the Atlantic offshore area, is projected to continue warming throughout the 21st century (IPCC 2013). However, the degree of warming varies across Canada (Natural Resources Canada 2016). Projections of future precipitation involve more uncertainties than temperature, and are generally of lower statistical significance than changes in temperature (Barrow et al. 2004). Although the annual total precipitation is projected to increase in the 21st century, because of enhanced evapotranspiration driven by warmer temperatures, many regions will experience a moisture deficit as well as low flow in the summer.

Global warming can potentially impact any country's future economic growth. There had been studies conducted to understand the atmosphere and hydrological process of Mackenzie River Basin (Woo et al. 2008), but there has been limited application of a mesoscale climate model to simulate the climatic processes of MRB (Mackenzie River Basin). The objective of the current study is to increase our understanding of the regional climate and sensitivity of the climate of MRB.

In this study, the mesoscale climate model called WRF was selected to simulate the climate of MRB for May, June, July and August, September, October (MJJASO) of historical period (1979-2005), and to dynamically downscale the climate projections of IPCC (2013) over the 2050s

(2041-2070). This effort using WRF will contribute to our understanding of the regional climatic and the local hydrological response of MRB to the potential impact of climate change.

CHAPTER THREE

RESEARCH METHODOLOGY

3.1 Earth's climate system

The Earth's climate system is influenced by solar radiation, wind, ocean current, and other factors. The incoming solar energy must be balanced by the outgoing radiation to keep the Earth's atmospheric temperature consistent. When the radiation emitted from the Earth's surface is absorbed by certain atmospheric constituents, it adds heat to the atmosphere. The climate system consists of five major components: the atmosphere, the hydrosphere, the cryosphere, the land surface and the biosphere, forced or influenced by various external forcing mechanisms. Changes of energy balance will lead to a new pattern of climate. Figure 10 shows the main components of Earth's atmospheric system that causes the change of energy balance and leads to climate change.

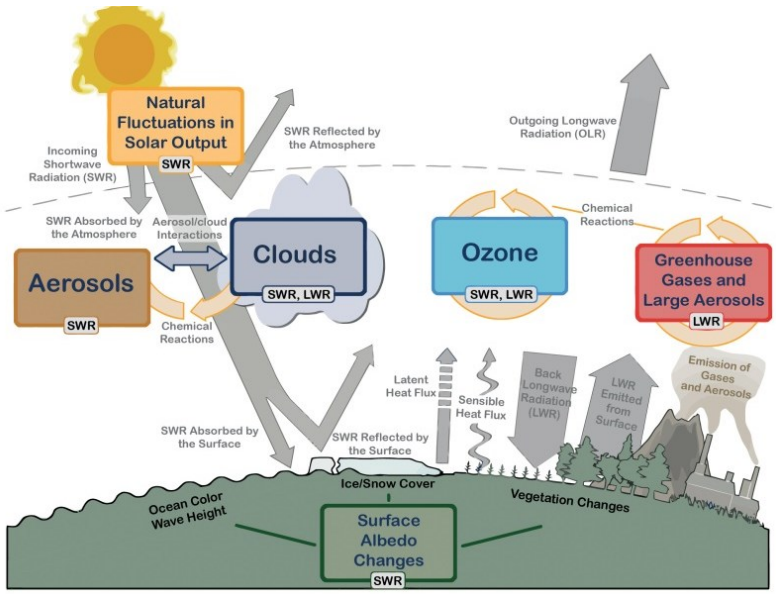

Figure 10: Main drivers of climate change (source: IPCC 2013)

3.2 Global and Regional Scale Climate

The elements of the global climate system, the individual components and processes are connected and influenced to each other in diverse ways. Global climate is usually defined as the average of global weather or the relevant quantities over a period of time ranging from months to several thousands of years. The focus quantities are surface variables such as temperature, precipitation and wind. By the definition of World Meteorological Organization, climate can be defined by averaging these variables over 30 years.

Regional climates are complex results of the global processes that vary with locations and have different response to those global-scale impacts. The global scale climate phenomena are well simulated by global climate models providing much better scientific basis for understanding and developing regional climate model. Understanding and the analysis of impact of future climate change on hydrological regimes is hindered by the discrepancy of scales between general circulation model outputs and the spatial resolution of the catchment-scale hydrological simulation models.

The General Circulation Models (GCMs) simulate global conditions with spatial scales of more than hundreds of kilometers, while much finer resolution data are required for simulating the basin hydrology. In order to incorporate the GCM simulations, the spatial and temporal scales of climate variables simulated by GCMs can be downscaled to regional scale. Figure 11 shows different conceptual horizontal grids of an example of a GCM and a RCM, and the grids of a hydrological model.

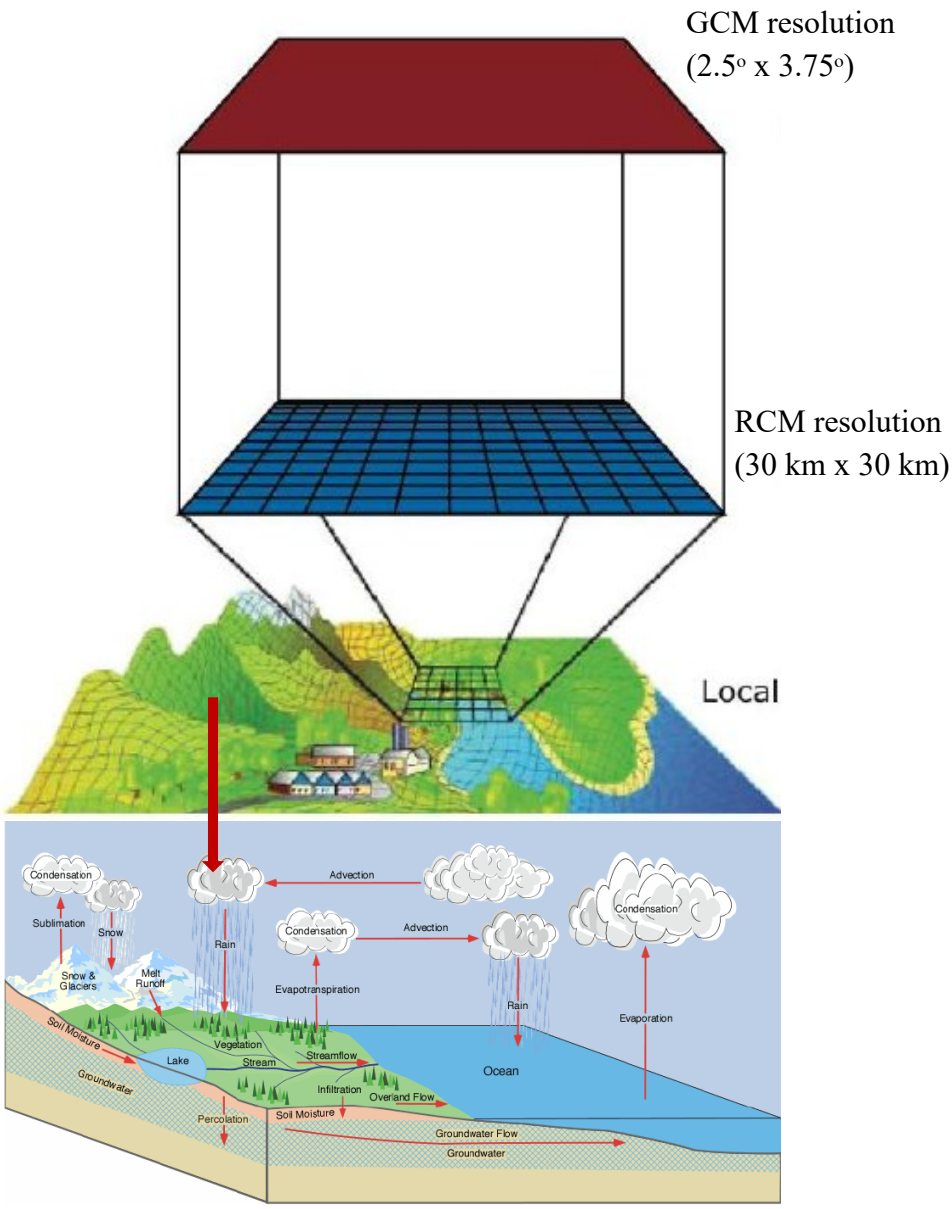

Figure 11: Typical horizontal grid resolutions of a GCM, a RCM and a distributed land surface scheme or a hydrologic model (Pidwirny 2006).

3.3 Climate Change Scenarios

According to IPCC (2013), "Climate change refers to a change in the state of the climate that can be identified (e.g., by using statistical tests) by changes in the mean and/or the variability of its properties, and that persists for an extended period, typically decades or longer". Climate change,

can lead to changes in the water and energy cycle and the likelihood of the occurrence or strength of extreme weather and climate events or both.

As reported by IPCC (2013) “future climate will depend on committed warming caused by past anthropogenic emissions, as well as future anthropogenic emissions and natural climate variability”. It has been concluded that the increase of global mean surface temperature in near future (2016–2035) will likely be in the range 0.3°C to 0.7°C relative to 1986–2005 for the four RCPs; in the 5th assessment report (IPCC 2013) the future climate scenarios adapted are RCPs “Representative Concentration Pathways" according to their 2100 radiative forcing level relative to the preindustrial values. The RCPs are four independent pathways developed by four individual modeling groups; The values (RCP 2.6, RCP 4.5, RCP 6.0 and RCP 8.5) followed by the RCP are proportioned to the greenhouse gas emission, starting from very low to high accordingly.

Relative to 1850–1900, global surface temperature change for 2081–2100 is projected to likely exceed 1.5°C for RCP4.5, RCP6.0 and RCP8.5 climate scenarios (Iacono et al. 2008). Warming is likely to exceed 2°C for RCP6.0 and RCP8.5 climate scenarios relative to 1986–2005 (Figure 12). Particularly, the air temperature of the Arctic will continue to warm more rapidly than other parts of the Earth. There will be more frequent hot and fewer cold temperature extremes over most land areas at daily and seasonal timescales and it is very likely that heat waves will occur with a higher frequency and longer duration (IPCC 2013).

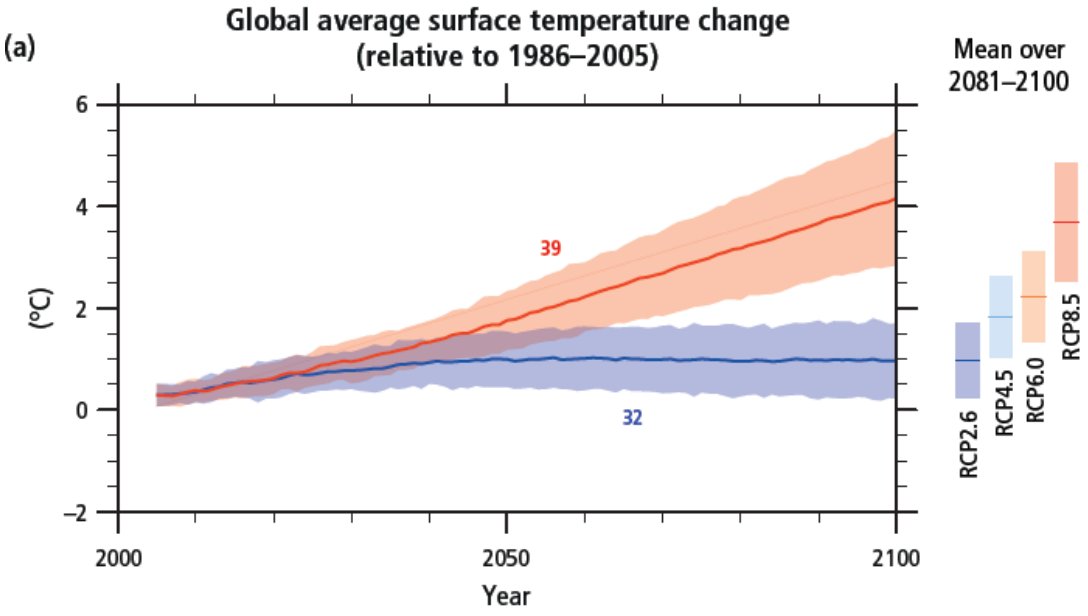

Figure 12: Global average surface temperature change from 2006 to 2100 as determined by multi-model simulations. All changes are relative to 1986–2005 (source: IPCC 2013).

3.4 Literature Reviews of Climate Change

According to the IPCC 5th assessment report, the precipitation changes will not be uniform all over the world; the high latitudes and the equatorial Pacific are likely to experience an increase in annual mean precipitation under the RCP8.5 climate scenario. In many mid-latitude wet regions, mean precipitation will likely increase under the RCP8.5 climate scenario. It is more likely that intensity and frequency of extreme precipitation events over most of the mid-latitude land masses and over wet tropical regions will increase.

Projected changes in the hydrologic cycle may have very significant impacts on the inhabitants. Changes in rainfall and temperature will impact the intensity and frequency of flooding, change the soil moisture condition and enhance the drought, and it could affect the navigability and water transportation of the some regions in Canada. “If society is not well prepared for such

changes and fails to monitor variations in the hydrologic cycle, large numbers of people run the risk of living under water stress or seeing their livelihoods devastated by water-related hazards such as floods" (Oki and Kanae 2006). It is important, therefore, to examine the influence of climate change especially at regional scales. Prediction of climate change is vital for mitigation, adaptation, and planning in various sectors of society, the economy, and the environment; knowing the magnitude of uncertainty associated with different aspects of prediction is important

3.5 Downscaling

Global climate models (GCMs) provide coarse resolution climate simulated and the details of the spatial features are not well preserved, which might not be sufficient to analyze the local scale of climate change. Since the regional model's domain usually covers smaller areas, it allows higher spatial resolution if the similar number of grid points was selected based on a GCM. The higher spatial resolution simulations improve the detailed analysis of climate change for the simulated region. On the other hand, regional climate modeling relies on information provided by the lateral boundaries and the initial conditions which can be obtained from GCMs. Regional climate are generally well simulated by a mesoscale model in relatively flat and homogenous terrain. Selections of model schemes are subject to the local climate as well as on the complexities of the terrain.

Downscaling is usually described as a procedure to simulate the local climate depending on the information provided at large scales, i.e. it is a method for generating high-resolution climate data from relatively coarse-resolution GCMs. The primary strategy is to connect the global scale climate to regional dynamics in order to generate specific regional climate. The two main approaches are statistical and dynamical downscaling.

3.5.1 Statistical downscaling

Statistical downscaling is a two-step process consisting of i) the development of statistical relationships between local climate variables (e.g., surface air temperature and precipitation) and large-scale predictors (e.g., pressure fields), and ii) using such relationships to obtain the local climate characteristics based on the GCM experiments. Examples of statistical downscaling methods are such as regression-based models, neural network models, Statistical Down-Scaling Model (SDSM); Automated Statistical Downscaling (ASD) tool; Support Vector Machine (SVM), and others.

3.5.2 Dynamical Downscaling

Dynamic downscaling involves using numerical meteorological modeling to reproduce local weather conditions based on global climate patterns through a regional climate model. Usually, dynamical downscaling involves physically based modeling which are computationally intensive. Outputs from GCM simulations are used to derive initial and time-varying (for example, 6-hour) lateral (vertical profiles of temperature, humidity, wind) and surface (pressure and sea surface temperature) boundary conditions for a three-dimensional model domain that is selected to capture the important synoptic- and mesoscale atmospheric circulation features that determine the climatology of a region of interest. The atmospheric processes are governed by laws of physics calculated by numerical methods. Dynamical downscaling of future climate at a finer resolution provides necessary information at the spatial scale necessary for climate change analysis and decision making for climate change adaptation.

3.6 Weather Research and Forecasting (WRF) model

The Weather Research and Forecasting (WRF) model was specifically designed for high resolution applications, and provides an ideal tool for assessing the value of high resolution regional climate modeling (Done et al. 2004). It could serve both atmospheric research and operational forecasting needs for any area (WRF Model Organization 2015). The WRF model is being used as a regional climate model (RCM) for dynamical downscaling of global model data in different parts of the world because WRF provides the freedom to select the options that best describe the regional climate of interest and produces finer resolution data (Prabha et al. 2011).

Several studies have been reported on applications of WRF model; Pérez et al. (2014) investigated the ability of the WRF Model simulations over a complex region, the Canary Islands. They found that the simulated maximum and minimum temperatures, together with the daily rainfall, were comparable with the ECMWF Re-Analysis (ERA-Interim) data. They also stated that both the microphysics and the boundary layer schemes have a large impact on the simulated precipitation. Zhang et al. (2012) found that the WRF model can realistically simulate the magnitude and geographical distribution of the mean rainfall over the Hawaiian Islands; in addition, their model simulations reproduced the individual heavy rainfall events well. They concluded that WRF can be a useful tool for dynamical downscaling of regional climate over the Hawaiian Islands.

Mooney et al. (2013) applied the Weather Research and Forecasting model (WRF) to downscale the interim ECMWF Re-Analysis (ERA-Interim) data for the climate over Europe for the period of 1990–95, they suggested that parameterization combinations should be carefully selected for

simulating realistic climate variables such as surface air temperatures (T2), precipitation, and mean sea level pressure (MSLP).

Gula and Peltier (2012) applied WRF model for Great Lakes system of North America and demonstrated that the more comprehensive physics option of WRF model provides significantly improved results compared to those obtained from the global model. The model showed a greater success to capture the details of the annual cycle and spatial pattern of precipitation as well as to produce much more realistic lake-induced precipitation and snowfall patterns. Zhang et al. (2013) suggested that WRF model is able to reproduce the weather phenomena and can forecast the near-surface variables well in flat terrain.

The Advanced Research WRF (ARW-WRF) Modeling system gives a large selection of physical parameterizations which makes the model more specified according to our need (WRF Users Page 2014). The selection of physics options depends on different factors like the type of output variables needed and input data available to run the model. The combinations of physics parameterizations are also influenced by the geographic position and topography of the area. There is no single combination of physics parameters that could be taken as the best option for a particular area without testing its sensitivity, because the general selection criteria of physics parameterizations only gives the preliminary idea but not the best results for that particular area. So a number of sensitivity tests may be required to get a single combination of physics that could produce comparable results for that area. WRF offers multiple physics options typically range from simple to sophisticate and more computationally costly (WRF Users Page 2014). Selection of physics parameterizations requires some understanding of the physical and climatic conditions of the area. For example, in a cold region, the selected physics parameterizations are expected to be different than that in the hot and humid region.

Microphysics, Longwave and Shortwave Radiation, Surface Layer, Land Surface, Lake Physics, Planetary Boundary layer, Cumulus Parameterization are the physics options that play an important role in simulating the regional climate (Pei et al. 2014; Pérez 2014; Mooney et al. 2013). Short description of physics options (tested by other researchers) that have potential applicability to MRB are discussed below:

WRF provides more comprehensive physics processes and choice of land surface schemes; the 5-layer thermal diffusion scheme using five layers soil temperature (Dudhia 1996). The Noah Land Surface scheme includes simulations of soil temperature and moisture in four layers, fractional snow cover and frozen soil physics. New modifications were added to represent processes over ice sheets and snow covered area (Tewari et al. 2009). The RUC Land Surface scheme includes simulations of soil temperature and moisture in six layers, multi-layer snow and frozen soil physics (Benjamin et al. 2004). It has been applied by researchers in different regions (Mooney et al. 2013).

For microphysics scheme, Lin et al. scheme is widely used (Pennelly et al. 2014) which is a sophisticated scheme with ice, snow and graupel processes, suitable for real-data high-resolution simulations. The WRF Single-Moment 3-class scheme is a relatively simple, efficient scheme with ice and snow processes suitable for mesoscale grid sizes (Hong et al. 2004) while the WRF Single-Moment 6-class schemes is slightly more sophisticated version of the previous one, allows for mixed-phase processes and super-cooled water (Hong et al. 2006). The Eta microphysics is simple efficient scheme with diagnostic mixed-phase processes for fine resolutions (< 5km).

The radiation schemes are an important part of the climate model (Figure 13). The WRF model provides different options for shortwave and longwave radiation estimations. The RRTM

longwave scheme (Rapid Radiative Transfer Model) is an accurate scheme using look-up tables for efficiency; it accounts for multiple bands, and microphysics species (Mölders et al. 2010). The CAM Shortwave and Longwave Schemes allow for aerosols and trace gases. New Goddard scheme is efficient with multiple bands, ozone from climatology (Chou and Suarez 1999) for both shortwave and longwave radiation. The Dudhia shortwave scheme is a simple downward integration allowing clouds and clear-sky absorption and scattering (Dudhia 1989).

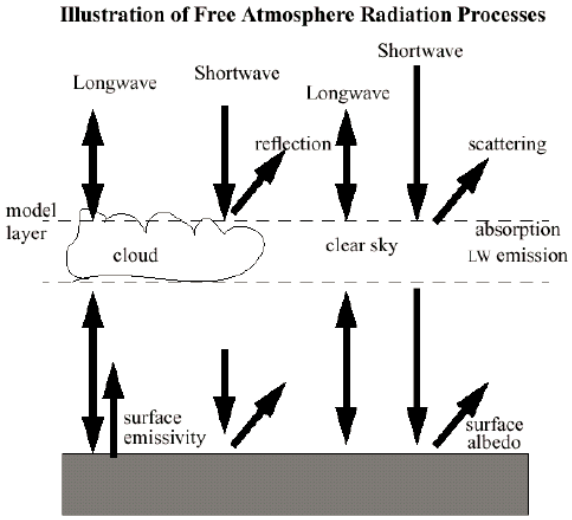

Figure 13: Illustration of atmospheric radiation process (Adapted from Dudhia 1989)

Several PBL schemes are available in the WRF model. The Yonsei University scheme applied by Flesch and Reuter (2012) is a Non-local-K scheme with explicit entrainment layer and parabolic K profile in unstable mixed layer (Hong et al. 2006). The Mellor-Yamada-Janjic scheme is a one-dimensional prognostic turbulent kinetic energy scheme with local vertical mixing. The Quasi-Normal Scale Elimination PBL used a new theory for stably stratified regions, daytime part uses eddy diffusivity mass-flux method with shallow convection.

For the Cumulus scheme, the Kain-Fritsch scheme, a deep and shallow convection sub-grid scheme using a mass flux approach with downdrafts and CAPE removal time scale, was applied by several researchers (Flesch and Reuter 2012); whereas the Betts-Miller-Janjic scheme is an operational Eta scheme. WRF model physics parameterization used in the experiments are given in Appendix A.2.

3.6.1 Land Surface Physics

Land surface plays a key role in the global energy budget, affects the redistribution of energy and thus contributes to the climatic system. In the global water cycle, soil moisture has a significant contribution to the exchange of moisture and heat between the atmosphere and the land surface. Soil moisture directly affects the evapotranspiration from the plants and evaporation from the soil surface, which influence of the atmospheric boundary layer.

Soil moisture, effects of snow cover, soil heat flux, thermal conductivity, surface emissivity/ albedo, canopy water content and the relationship between the land surface and the atmosphere are established in a land surface model. Different Land Surface Models have been developed starting from the early 1960's to the recent year.

In the WRF model configuration, different Land Surface Model schemes are available to couple with the WRF model scheme. It is required to select a land surface model which could realistically capture the surface phenomenon of the region. Figure 14 illustrates the Surface Process of energy balance. In this study we primarily tested three Land surface Models in combination with the other physics parameterizations. They are discussed below:

5–layer Thermal Diffusion Scheme

It is a relatively simple model which can predict soil temperature but soil moisture availability is based on land use only. It provides heat and moisture fluxes for PBL.

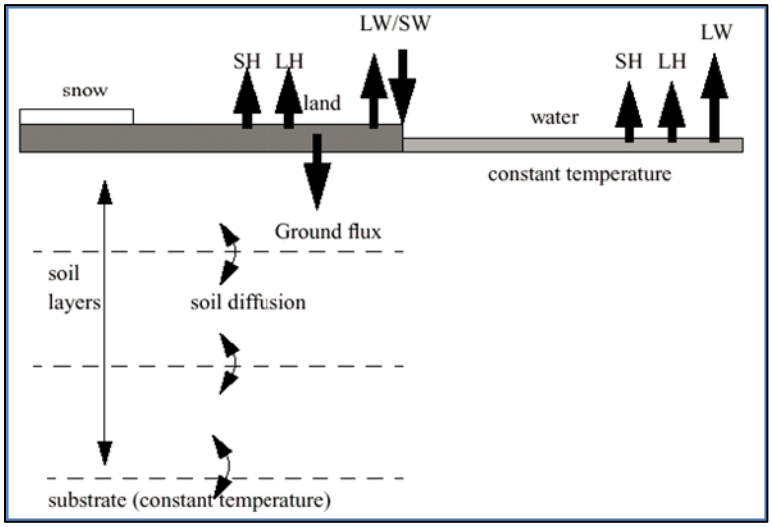

Figure 14: Illustration of Surface Process of energy balance (Adapted from Dudhia 1989)

Noah Land Surface Model

Fig. 15 illustrates the conceptual unified Noah land surface model structure. The unified Noah LSM was developed as a result of collaborative effort among NCEP, NCAR, AFWA and OSU (Tewari et al. 2009). National Centers for Environmental Prediction (NCEP) utilizes the Noah land surface model (Livneh et al. 2010) in the numerical weather and climate prediction models. Noah Land Surface Model treated the soil temperature and moisture into four layers. The unified Noah LSM is designed for high-resolution real time weather forecast, air pollution, local and regional hydrologic applications and the model comes efficient as well as relatively simple (WRF User Page 2007). In the Weather Research and Forecasting (WRF) model, Noah provides

improved Physics for frozen-ground and patchy snow cover. Better Soil heat flux treatment under snow pack and seasonal surface emissivity is included in the Noah LSM.

The model uses a bulk surface layer with a single (dominant) vegetation class and snowpack, overlying a (dominant) soil texture divided into four layers. The vegetation canopy is assumed to cover a fraction of the land surface that varies spatially and temporally by an input greenness fraction derived from the photosynthetically active portion of leaf area index (LAI), and based on monthly 5-yr climatology of Advanced Very High Resolution Radiometer (AVHRR) satellite data. The remainder of the grid cell is bare soil. Water can be intercepted by the vegetation canopy up to a prescribed maximum threshold. The soil temperature profile is determined using nonlinear functions for the thermal conductivity of each soil layer. Both of these computations require parameters such as porosity, wilting point, dry density, and quartz content that relate to soil texture. The model does not explicitly form a water table and capillary rise does not occur in the strict sense but rather as the result of vertical dispersion via the solution to the Richards equation. Infiltration into the soil follows as a nonlinear function of soil saturation, bounded above by precipitation and below by soil hydraulic conductivity. Sensible heat flux and ground heat flux are computed by the thermal diffusion equation, as differences between skin and air temperatures and soil and skin temperatures, respectively, whereas latent heat flux is a function of the actual ET. In the absence of snow, ET occurs either by canopy evaporation, bare soil evaporation, or transpiration through the root zones.

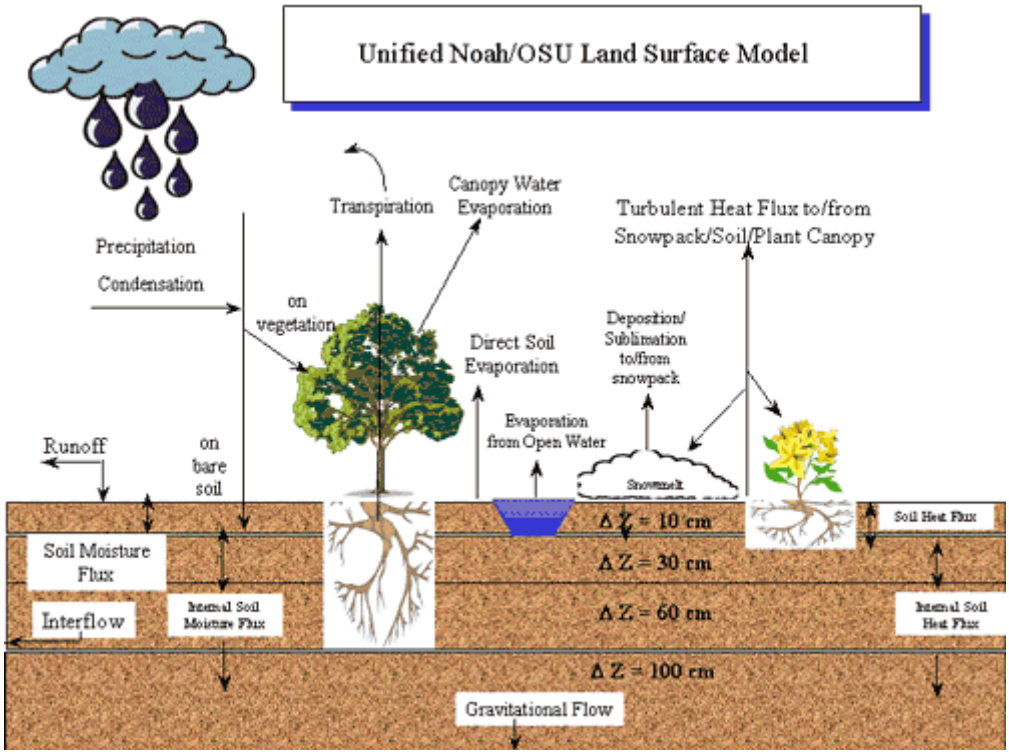

Figure 15: The Conceptual Unified Noah Land Surface model structure
(source: Research Application Laboratory 2015)

The Noah snow model prescribes a seasonally varying snow albedo decay function and provides for liquid water retention within the snowpack and partial snow coverage. Frozen soil physics provides for a reduction in moisture movement in response to increased soil ice content. Further details of the Noah snow model can be found in Livneh et al. (2010).

RUC Land Surface Model

The RUC LSM contains a multilevel soil model, treatment of vegetation, and a two-layer snow model, all operating on the same horizontal grid as the atmospheric model. The energy and moisture budgets are applied to a thin layer spanning the ground surface and including both the soil and the atmosphere with corresponding heat capacities and densities (Figure 16). The RUC

frozen soil parameterization considers latent heat of phase changes in soil by applying an apparent heat capacity, augmented to account for phase changes inside the soil, to the heat transfer equation in frozen soil in place of the volumetric heat capacity for unfrozen soil. The effect of ice in soil on water transport is also considered in formulating the hydraulic and diffusional conductivities of precipitation at the surface, as well as its partitioning between liquid and solid phases, is provided by the mixed-phase cloud microphysics routine. With or without snow cover, surface runoff occurs if the rate at which liquid phase becomes available for infiltration at the ground surface exceeds the maximum infiltration rate. The solid phase in the form of snow or graupel (treated identically by the LSM) is accumulated on the ground/snow surface to subsequently affect soil hydrology and thermodynamics of the low atmosphere. The most recent version of the LSM implemented in the RUC20 has a number of improvements in the treatment of snow cover over those described in Smirnova et al. (2004). Figure 16 shows the conceptual RUC Land Surface model structure.

The RUC model allows evolution of snow density as a function of snow age and depth, the potential for refreezing of melted water inside the snowpack, and simple representation of patchy snow through reduction of the albedo when the snow depth is small. If the snow layer is thinner than a 2-cm threshold, it is combined with the top soil layer to permit a more accurate solution of the energy budget. This strategy gives improved prediction of nighttime surface temperatures under clear conditions and melting of shallow snow cover.

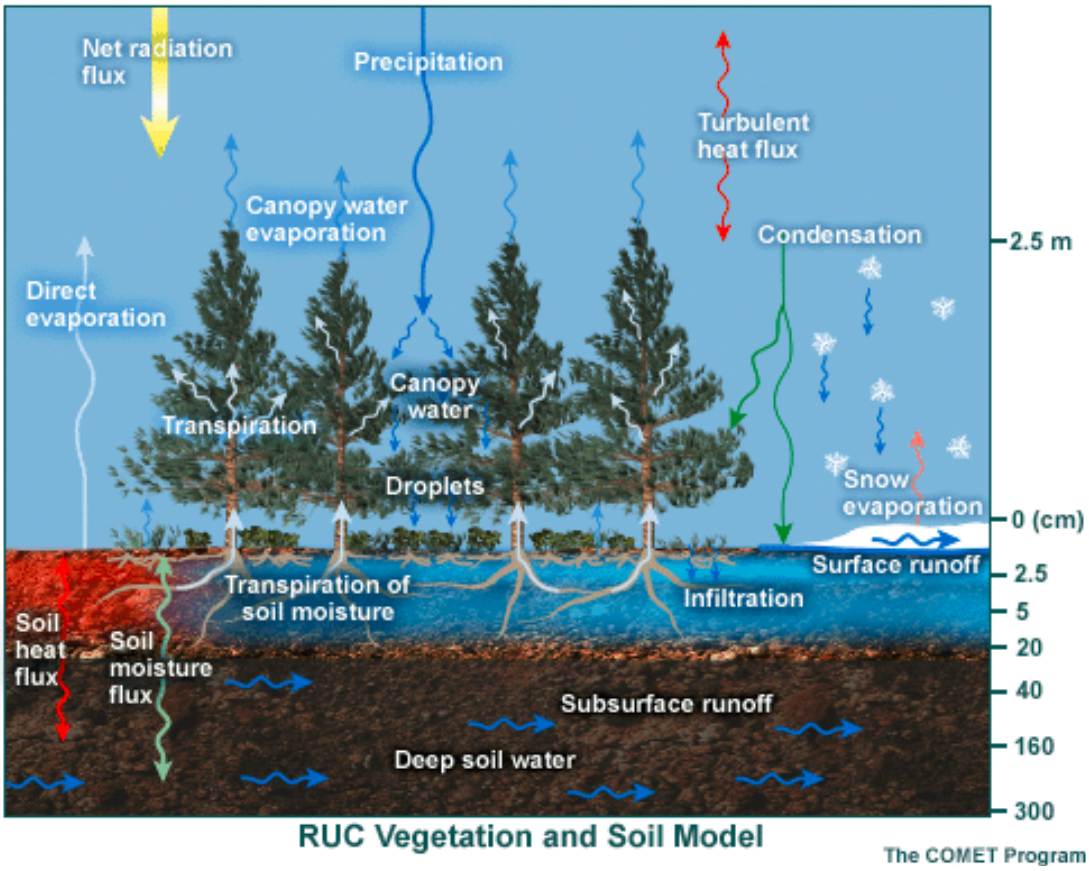

Figure 16: The Conceptual RUC Land Surface model structure (source: NOAA Earth System Research Laboratory 2015)

In applications of the RUC LSM in current and previous versions of the RUC, volumetric soil moisture and soil temperature at the six soil model levels, as well as canopy water, snow depth, and snow temperature are cycled. In the RUC20, cycling of the temperature of the second snow layer (where needed) is also performed. The RUC continues to be unique among NCEP operational models in its specification of snow cover and snow water content through cycling. The two-layer snow model in the RUC20 improves the evolution of these fields, especially in springtime, more accurately depicting the snow melting season and spring spike in total runoff.

3.7 The WRF Modeling System Program Components

WRF Modeling System consists of these major programs:

The WRF Preprocessing System (WPS)

The WRF Preprocessing System (WPS) is a set of three programs whose collective role is to prepare input to the real.exe program for real-data simulations. Each of the programs performs one stage of the preparation: *geogrid* defines model domains and interpolates static geographical data to the grids; *ungrib* extracts meteorological fields from GRIB-formatted files; and *metgrid* horizontally interpolates the meteorological fields extracted by ungrib to the model grids defined by geogrid.

ARW solver

The WRF model is a fully compressible and nonhydrostatic model (with a run-time hydrostatic option). Its vertical coordinate is a terrain-following hydrostatic pressure coordinate. The WRF model code contains several programs including numerical integration program (*wrf.exe).* The WRF model, Version 3.6.1, supports a variety of capabilities.

Post-processing & Visualization tools

There are a varieties of visualization tools available to display and analyze WRF outputs (WRF Model Organization 2015). The available post-processing utilities are NCL, RIP4, ARWpost (converter to GrADS and Vis5D), and WPP.

The components of WRF model system are shown in APPENDIX A.1.

3.7.1 Horizontal and vertical grids in WRF

For the horizontal grid plane, the WRF-ARW uses Arakawa-C grid staggering. For this configuration, the U component of the wind is located on the left and right side while the V

component is located on the top and bottom of each cell. All scalar quantities such a temperature, density and vapor mixing ratios are located in the center cell. The vertical coordinate system can also be referred to as the traditional sigma or mass vertical coordinate system. The terrain-following hydrostatic pressure vertical coordinate is denoted by η and is shown as Figure 17.

Map projections used for the WRF-ARW's domain depends on its location and size; the Lambert conformal projection is widely used, since this projection system best preserves lines of latitude and longitude. The location of the coarse domain is determined using the center of the coarse domain, the ref_lat and ref_lon variables (WRF Users Page 2014).

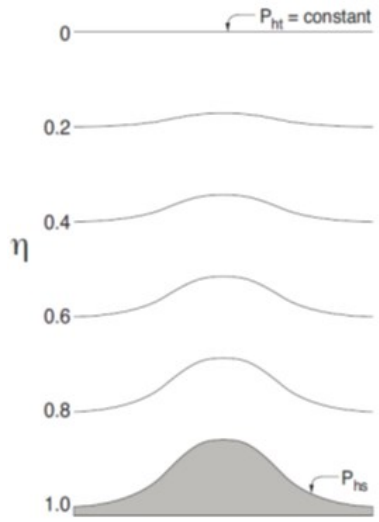

Figure 17: Eta vertical coordinate system (source: WRF Users Page 2014)

3.8 Data Sets

WRF model requires climate and geographical data for setting up the initial condition and the boundary conditions. The common input variables are temperature, U and V wind, Geopotential

height, mean sea level pressure, surface pressure, specific humidity, sea surface temperature, ice cover, soil temperature, and soil moisture etc.

Historical climate data source

The ERA-Interim reanalysis data are third generation reanalysis products which are spatially and temporally complete data set of multiple variables at high spatial and 6-h temporal resolution. These are global atmospheric reanalysis data sets, available from 1979 to the recent date in the European Centre for Medium-Range Weather Forecasts (ECMWF 2015) data server. ECMWF data are originally produced at model levels (hybrid pressure-sigma coordinates) and at the surface. Other levels such as pressure levels, isentropic levels for some datasets include data. The spatial resolution of the data set used in this study is 1 degree by 1 degree resolution. The ERA-Interim data were used in both calibration and validation phase of WRF modeling.

ANUSPLIN data (daily 10 km gridded) and the "Second Generation of Daily Adjusted Precipitation for Canada" was collected from Environment Canada are used for assessing the performance of the dynamically downscale climate data over the Mackenzie River Basin.

GCM Climate Data

The historical and 2041-2100 simulations under RCP 8.5 and RCP 4.5 climate scenarios using CanESM2 (the second generation of Earth System Model) data were collected. The CanESM2 is the fourth generation coupled global climate model developed by the Canadian Centre for Climate Modelling and Analysis (CCCma) of Environment Canada. The CanESM2 also represents the Canadian contribution to the IPCC Fifth Assessment Report (AR5). The 128x64 grid cells cover global domain using T42 Gaussian grid. This grid is uniform along the longitude with horizontal resolution of 2.8125° and nearly uniform along the latitude of roughly 2.8125°.

Streamflow Data

Streamflow data were obtained from the hydrometric database (HYDAT) of Environment Canada (2013). River stage and discharge data at selected stations were also collected from the Water office Canada (2015). High resolution Digital Elevation Model (0.75 arc second) data for the Mackenzie River Basin were collected from the University of Alberta Library resources and also from the USGS HydroSHEDS web site.

3.9 WRF Model Parameterization

The Weather Research and Forecasting (WRF-ARW) model version 3.6.1 was used to dynamically downscale global climate data over the MRB. Summer of 2009 (MJJA) was selected as the testing period. The domain was selected as shown in Figure 18, so that the MRB gets required freedom to develop its own synoptic and mesoscale circulation. Selecting a large domain could be very expensive in terms of computing memory and resources. Since MRB is the largest river basin in Canada, occupies about 1.8 million square km, so selection of an optimum domain size was critical. After several trials, the domain size was selected with 180 grids in east-west direction and 150 grids in north-south direction, where each grid cell is 30 km by 30 km in horizontal resolution with Lambert Conformal projection. Fig.18 shows the selected domain, which extends approximately from 42 °N to 72 °N and 90 °W to 150 °W. For the model setup and data preprocessing, the USGS 24-category land data were used. For the initial and boundary conditions of the WRF model runs, the ERA-Interim 1° degree by 1° degree data with 6 hourly time steps were used. The model was setup with 28 eta levels, they are as follows: 1.000 , 0.990 ,

0.978 , 0.964 , 0.946 , 0.922 , 0.894 , 0.860 , 0.817 , 0.766 , 0.707 , 0.644 , 0.576 , 0.507 , 0.444 , 0.380 , 0.324 , 0.273 , 0.228 , 0.188 , 0.152 , 0.121 , 0.093 , 0.069 , 0.048 , 0.029 , 0.014 , 0.000.

For the model physics parameter setup, three Land Surface model were tested. The first group is based on the sf_surface_physics option 1, which is the *5–layer Thermal Diffusion Scheme*. Table 1 shows different combinations of physics parameterizations considered in this study. Detailed description of the physics parameters used in this study are provided in details in Appendix A.2.

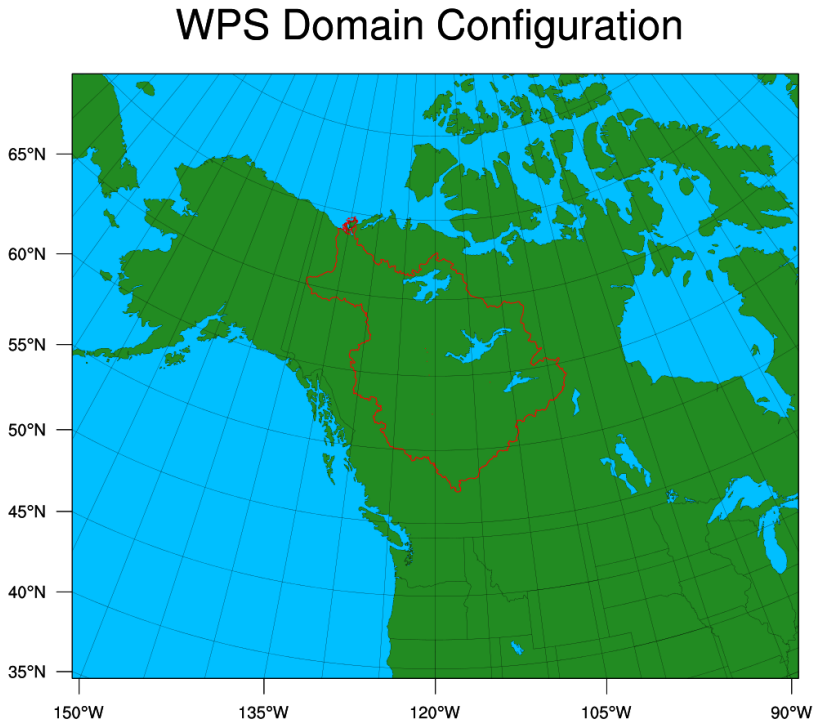

Figure 18: WPS domain configuration

For the second category the Unified Noah Land Surface Model was chosen as the Land Surface scheme, where total of 12 different combinations of physics parameters were tested with this option. Table 2 shows different combinations of physics parameterizations of WRF coupled to the Unified Noah Land Surface Model. Table 3 shows parameterizations using RUC Land Surface Model.

Table 2: Physics parameterization used with 5–layer Thermal Diffusion Scheme (sf_surface_physics=1)

Test No.	mp_physics	ra_lw_physics	ra_sw_physics	sf_sfclay_physics	bl_pbl_physics	cu_physics
1	3	1	1	1	1	1
2	4	4	4	1	1	1
3	2	4	4	1	7	1

Table 3: Physics options used with Unified Noah Land Surface Model (sf_surface_physics=2)

Test No.	mp_physics	ra_lw_physics	ra_sw_physics	sf_sfclay_physics	bl_pbl_physics	cu_physics
4	2	5	5	1	1	1
5	3	5	5	1	1	1
6	3	4	4	1	1	1
7	3	1	1	1	1	1
8	3	3	3	1	1	1
9	2	3	3	1	1	1
10	2	4	4	2	2	1
11	16	3	3	1	1	1
12	6	3	3	1	1	1
13	1	7	7	10	10	6
14	4	4	4	2	2	2
15	2	1	1	1	1	2

Table 4: Physics options used with RUC Land Surface Model (sf_surface_physics=3)

Test No.	mp_physics	ra_lw_physics	ra_sw_physics	sf_sfclay_physics	bl_pbl_physics	cu_physics
16	3	3	3	1	3	1
17	3	7	7	1	3	1
18	1	4	4	1	3	1

The current study focused on the above mentioned three land surface schemes, where 18 tests were performed to select the physics parametrization that produces comparable results for simulating the climate of Mackenzie River Basin.

3.10 HBV Hydrologic Model

A conceptual hydrologic model was used to simulate the stream flow of selected stations of the Mackenzie driven by the WRF model output data (temperature and precipitation). HBV is a conceptual semi-distributed, rainfall-runoff model that has been used to perform impact studies for various climate change assessments (Vehviläinen and Huttunen 1997; Bergstrom et al. 2001; Andréasson et al. 2004). The model typically operates on a daily time steps. Input data to HBV include precipitation, temperature and potential evapotranspiration data.

In this study climate data such as precipitation and temperature were calculated as a weighted mean of climate stations in and around the basin. Thiessen polygon method was used to determine the relative weight of different stations. When gridded climate data is used, an areal average is obtained. Hamon's (1961) temperature-index potential evapotranspiration equation was used to transform air temperature to potential evaporation as one of the model inputs (Eq. 1).

$$\mathrm{PET} = \frac{29.8 \times \mathrm{D} \times \mathrm{e_s}}{\mathrm{T}+273.3} \qquad (1)$$

Where $e_s = 0.611 \times e^{\frac{17.27T}{T+237.3}}$, PET is the potential evapotranspiration (mm/day), D, daylight hours (hrs), T is the mean daily temperature (°C) and e_s is the saturation vapor pressure (kPa).

The snow module of HBV uses a degree-day method to estimate snow accumulation and snowmelt processes. Precipitation is only considered as rainfall when the air temperature is above a threshold temperature *TT* ($^{\circ}$C), otherwise it is treated as snowfall. The amount of

snowfall is corrected by multiplying the data by a snowfall correction factor, *SFCF*. Based on the degree-day method, the amount of snowmelt, *M* (*mm day*$^{-1}$), and the amount of refreezing liquid water within the snow pack, *R* (*mm day*$^{-1}$), are computed from Eq. 2 and 3, respectively:

$$M = CFMAX \cdot (T(t) - TT) \tag{2}$$

$$R = CFR \cdot CFMAX \cdot [TT - T(t)] \tag{3}$$

Where *CFMAX* is the degree-day melt coefficient (*mm day*$^{-1}$ $^{\circ}C^{-1}$), *T* (*t*) the air temperature, and *CFR* the refreezing coefficient. The amount of rainfall and snowmelt is assumed to remain within the snowpack until the amount exceeds a fraction, *CWH*, of the snow water equivalent.

The soil moisture module of HBV is based on three empirical parameters: β, *FC* and *LP* where β controls the contribution of Input (*I*(*t*)) in mm, which consists of precipitation and snowmelt, the runoff response ($Q_S(t)$) and the contribution of ($I(t)$- $Q_S(t)$) to the soil moisture storage ($S_{sm}(t)$). *FC* (*mm*) that represents the maximum soil moisture storage (capacity for storing soil moisture) of the river basin is related to β by

$$\mathrm{Q_s(t)} = \left[{\mathrm{S_{sm}(t)}}/{\mathrm{FC}} \right]^{\beta} \cdot \mathrm{I(t)} \tag{4}$$

Excessive water from precipitation and snowmelt is transformed by the runoff response function (Eq. 4) to $Q_S(t)$. $LP \times FC$ controls the actual evapotranspiration (E_a) such that when the soil moisture, $S_{sm}(t)$, exceeds $LP \times FC$, $E_a = E_p$ (potential evapotranspiration, E_p) but if $S_{sm}(t)$ drops below $LP \times FC$, E_a will be reduced as shown in Eq. 5.

$$E_a(t) = \begin{cases} \frac{E_p(t) \cdot S_{sm}(t)}{LP \times FC} & S_{sm}(t) \leq LP \times FC \\ E_p(t) & S_{sm}(t) > LP \times FC \end{cases} \tag{5}$$

The runoff response functions and the model structure of HBV are shown in Figure 19. The model consists of two conceptual storages (tanks) that simultaneously re-distribute the generated runoff in terms of quick and slow responses, respectively. The recharge from the soil routine is divided into two parts. The portion of the recharge that is added to the upper tank is given by the parameter *PART*. The upper tank runoff, $Q_u(t)$, is assumed to be the lesser value of the upper tank storage, *SUZ* (mm) and $K_1 \cdot SUZ^{(1+\alpha)}$ (mm). Where α is a non-linearity coefficient and K_1 (day^{-1}) is a recession coefficient, which represents the basin's quick runoff responses:

$$Q_u(t) = \min(K_1 \cdot SUZ^{(1+\alpha)}, SUZ) \tag{6}$$

The remaining discharge generated in one day is distributed evenly over the subsequent period defined by the *DELAY* (day) parameter. The product of the lower tank storage *SLZ* (mm), and the recession coefficient K_2 (day^{-1}) is the lower tank runoff, $Q_l(t)$ given as

$$\mathrm{Q_l(t)} = \mathrm{K_2} \cdot \mathrm{SLZ} \tag{7}$$

The runoff from both tanks $Q_{ul}(t) = Q_u(t) + Q_l(t)$ is further transformed by a triangular weighting function:

$$\mathrm{Q_{sim}(t)} = \sum_{\mathrm{i=1}}^{\mathrm{MAXBAS}} \mathrm{c(i)} \cdot \mathrm{Q_{ul}(t - i + 1)} \tag{8}$$

where $c(i) = \int_{i-1}^{i} \frac{2}{MAXBAS} - |u - \frac{MAXBAS}{2}| \cdot \frac{4}{MAXBAS^2} du$

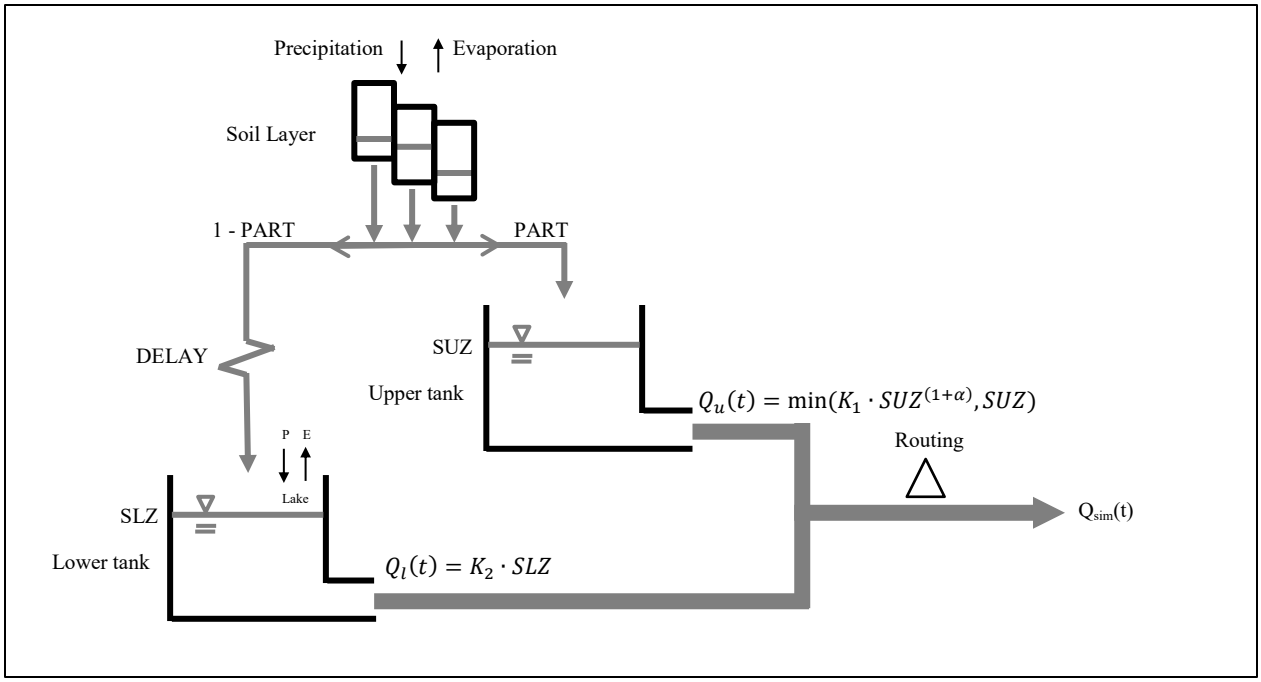

Figure 19: Model structure of the HBV model (modified from HBV Help Manual)

The Monte Carlo procedure entails performing a large number of simulations, and each individual simulation is allocated random parameter values from pre-defined parameter ranges. The other two HBV model parameters, CFR and CWH are set at 0.05 and 0.1, respectively as recommended, instead of being calibrated. Optimal values are fine-tuned using an objective function based on the Nash-Sutcliffe (NS) coefficient (Nash and Sutcliffe 1970) (Eq. 9) that essentially minimizes differences between the simulated runoff of HBV with observed streamflow. The calibrated HBV parameters are then validated using data independent of the calibration period.

$$NS = 1 - \frac{\sum_{t=1}^{n}\left(Q_o(t) - Q_{sim}(t)\right)^2}{\sum_{t=1}^{n}(Q_o(t) - \bar{Q})^2} \quad (9)$$

Where $\bar{Q}$ is the average streamflow, $Q_o(t)$ the observed streamflow, and n the data length.

Streamflow Rating Curves

Tables relating stage and discharge data at several gauging stations for the Mackenzie were obtained from the Water Survey of Canada, Environment Canada. Best-fit nonlinear regression equations developed from the stage-discharge data will be applied to convert simulated future discharge values to future river stages in meters. For the Fort Simpson station of the Mackenzie River, a table was provided for a river stage ranging from 1 m to 10.28 m at 0.01 m increments. At the Arctic Red River station, the corresponding table is of a stage ranging from 1.3 m to 9.50 m at 0.01 m increments. Figure 20 illustrates the Stage discharge relationships at Fort Simpson and Arctic Red River Stations.

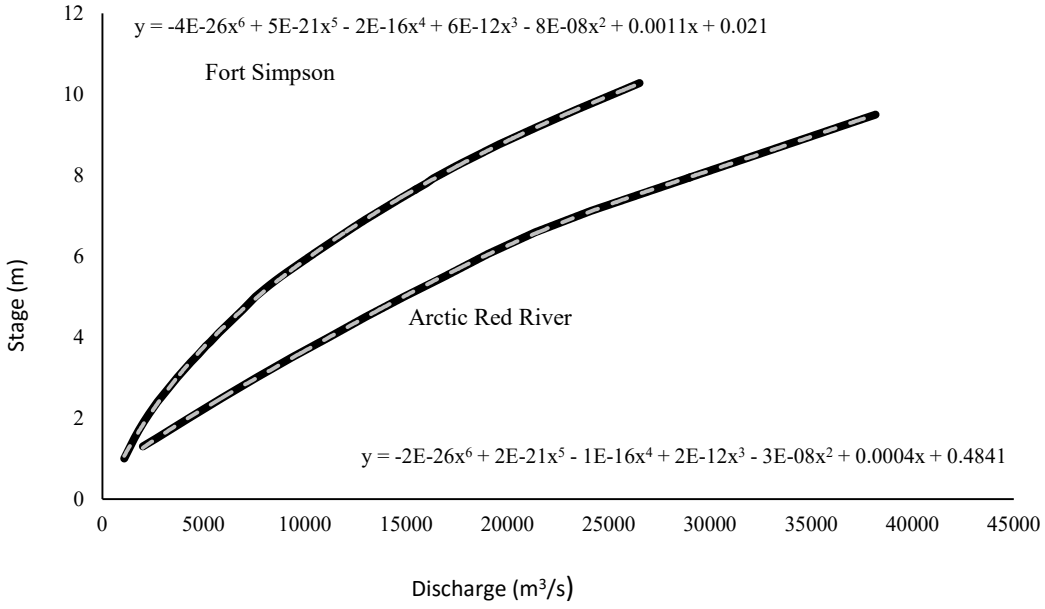

Figure 20: Stage discharge relationships at Fort Simpson and Arctic Red River Stations

CHAPTER FOUR

DISCUSSION OF RESULTS

4.1 Configuration of WRF Regional model

The accuracy of the regional climate of MRB simulated by WRF depends largely on how representative is the model configuration set up for the regional land and atmospheric processes of MRB, the selection of model parameters that are representative to physical and climatic factors such as topographic characteristics of the area, dominant climatic regime, circulation patterns, vegetation covers, etc.

The Mackenzie River Basin is the major regional, northern river basin of Canada with complex hydroclimatology. Daily precipitation and temperature data derived from eighteen sets of simulations of WRF driven by boundary conditions of ERA-Interim reanalysis data are compared with the climate station and gridded ANUSLPIN data of Environment Canada. A Taylor's diagram was used to statistically summarize the WRF outputs and their correlation, root-mean-square difference, and ratio of their variances with the observed data (Taylor 2001).

About 50 sets of model parameters were considered while we attempt to fine tune the physical parameterizations of WRF modules to capture the climate of MRB. Our model experiments show that the Land Surface Physics, Microphysics and Radiation Physics of WRF are sensitive to model the climate of MRB. A total of 18 WRF test runs were performed to test different combinations of model parameters as our effort to fine tune WRF to simulate realistic climate of the Mackenzie River Basin for the summer of 2009 as the testing period. The performance of

WRF was assessed by comparing its simulated rainfall and temperature data with different sets of reference data.

4.1.1 Temperature

Again, 18 different sets of 2-m temperature data were simulated by WRF using different WRF setups (table 3.1, table 3.2 and table 3.3), averaged over MMJA for 2009 and compared with the ANUSPLIN temperature data which are of 10-m horizontal resolution with daily time steps. WRF's simulated temperature data were re-gridded to the grid resolution of ANUSPLIN to estimate the temperature bias.

For the first test category (test # 1 to 3), it is observed that with a *5–layer Thermal Diffusion* scheme the temperature is well simulated, even though the bias of test # 1 could be up to -5° C in the lake region; while tests # 2 and 3 show 1 to 3°C positive bias in the lake region and slightly negative bias (up to -1 °C) in the north-western part of MRB. Figure 21 shows 2 m summer temperature bias (WRF-ANUSPLIN) over the MRB for the test period (MJJA 2009). Apparently, using the *Unified Noah Land Surface Model* with other physics schemes (test category 2) shows relatively high temperature bias. Tests # 4 to 10 have positive bias of up to 5 °C at the north-eastern part of MRB excluding the lakes. In the middle part of MRB, the positive bias tends to decrease gradually to become slightly negative bias over the mountainous area of MRB. Test # 8, 11 and 12 simulated better 2 m temperature, specially test # 11 and 12. For the third test category (experiment 16, 17 and 18), only experiment # 18 simulated reasonable temperature, while experiment # 16 and 17 simulated high temperature bias (WRF-ANUSPLIN) for MJJA 2009.

From Figure 21, the temperature bias tends to decrease from the western to eastern parts of MRB. The distribution of temperature shows that warm wind from the south-east extends over the central region, while colder temperature over the mountainous region extends to further north. This general spatial distribution of temperature has been successfully captured by WRF, even though WRF under simulated the mountain temperature and over simulated the central region with respect to ANUSPLIN data.

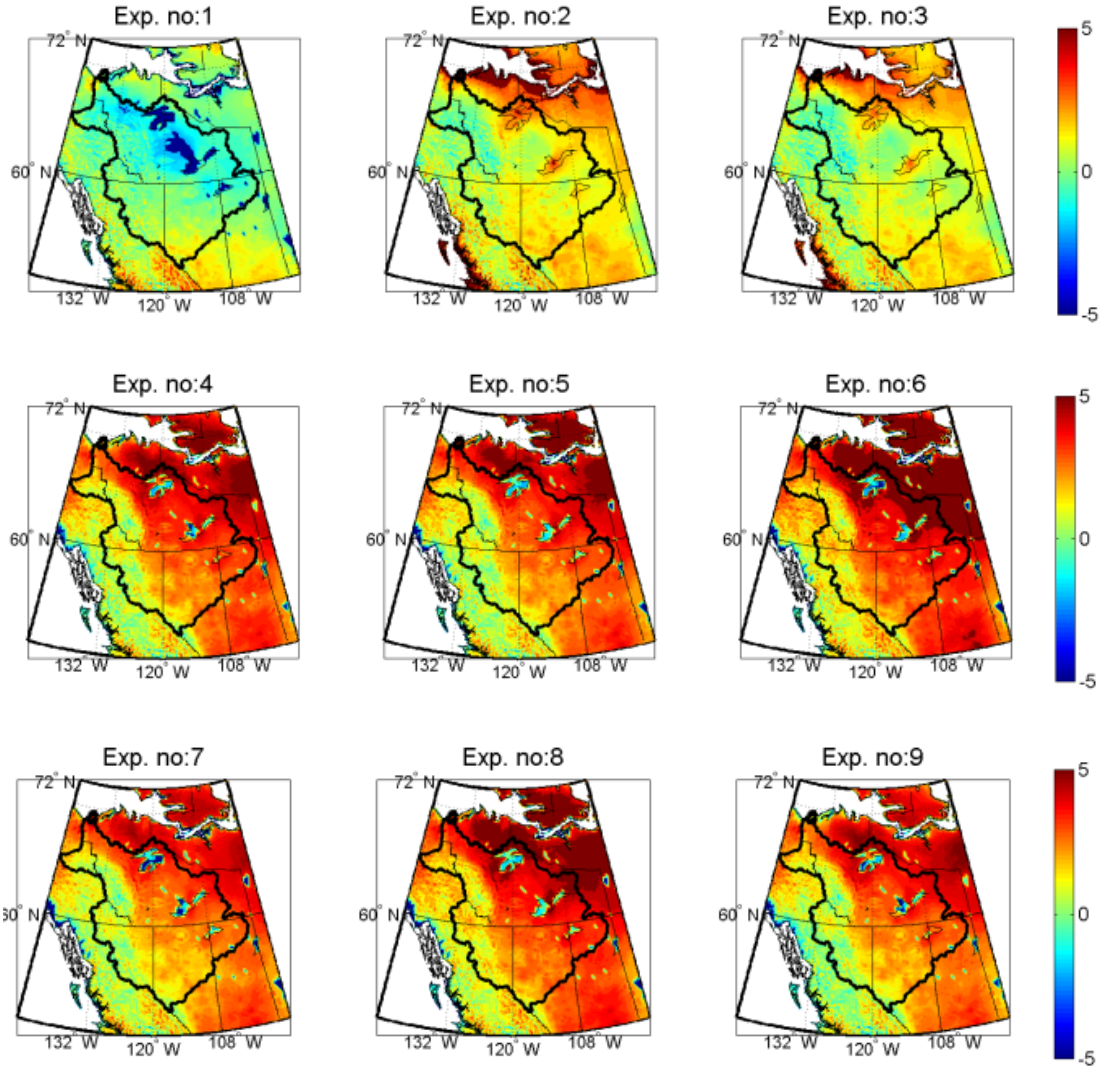

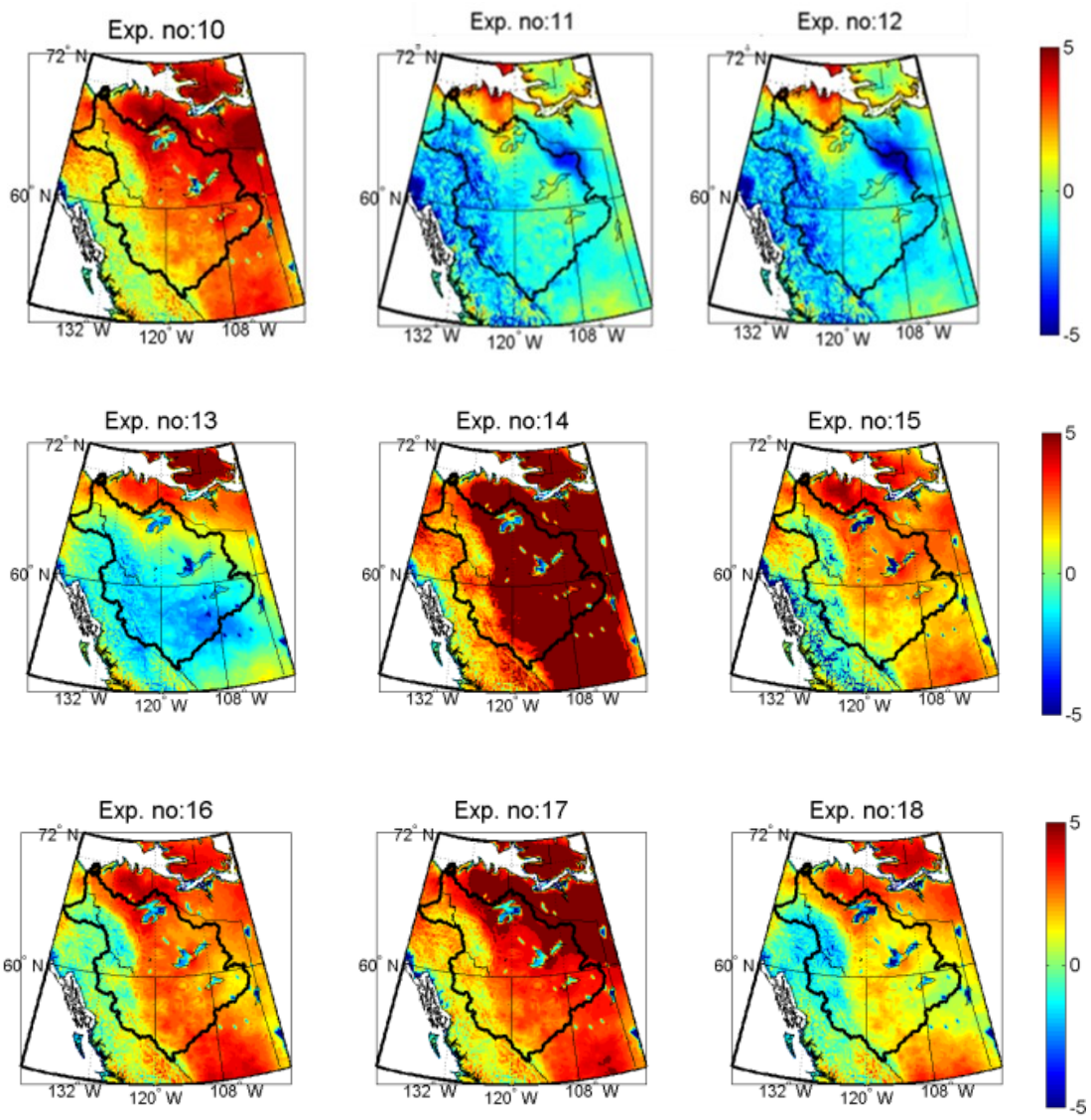

Figure 21: 2 m air temperature bias (WRF-ANUSPLIN) over MJJA of 2009 as the testing period for 18 test cases, test # 1 to test # 18, respectively.

Among the 18 sets of WRF's simulated 2-m air temperature based on the ERA-Interim data, only test # 11 and 12 have results comparable to that of ERA-Interim data.

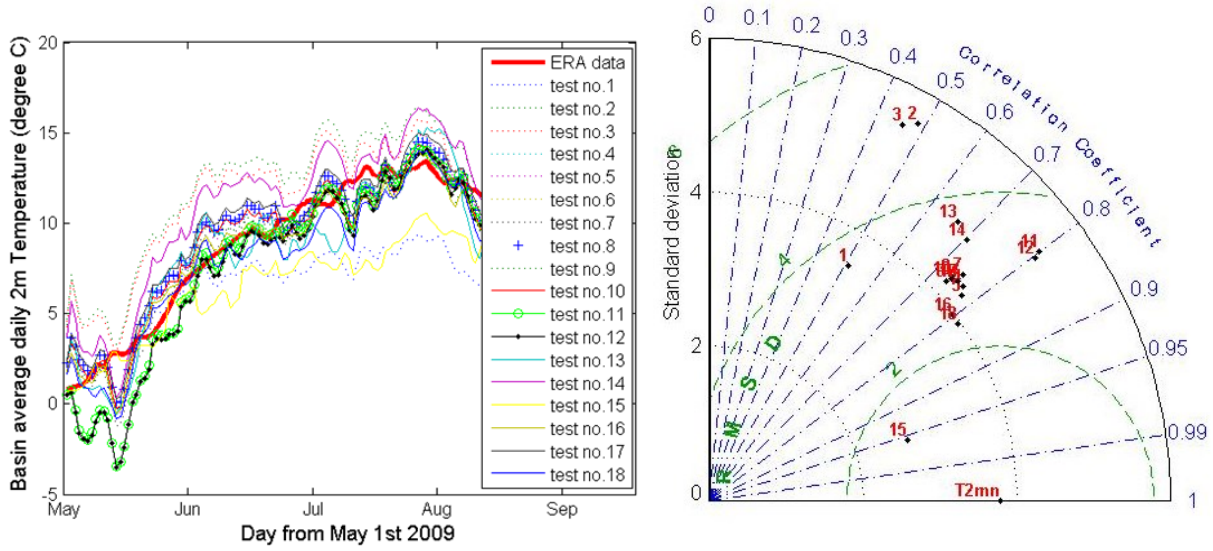

(a) (b)

Figure 22: (a) Average 2 m temperature over the MRB for MJJA 2009; b) Taylor diagram plot using the wrf experiments (experiment no. 1 to 18) and ERA-Interim data at 0.5x0.5 grid

Figure 22 (a) compares between ERA-Interim 2 m temperature data and WRF's simulated data using a Taylor diagram (Taylor 2001) to find their correlations. Figure 22(b) shows the correlation, RMSE, and standard deviation for eighteen sets of simulation over MRB of which experiment # 11 and 12 have good correlations (0.8), especially 11 based on the Unified Noah land surface model along with the WRF Double–moment 6–class Scheme, CAM shortwave and longwave schemes, Yonsei university scheme (YSU) for planetary boundary layer, and the Kain–Fritsch Scheme.

In summary, it seems setting up WRF using the Noah Land Surface model, the CAM Shortwave and Longwave Schemes, MM5 Similarity Surface Layer Scheme, with the WRF Single–moment or Double–moment 6–class microphysics Scheme will lead to simulated temperature that are comparable with ANUSPIN and ERA-Interim data over MRB. This agrees with the finding of

Mooney et al. (2013), who simulated the summer temperature over the Iberian Peninsula using different combinations of physics. They concluded that combining the CAM longwave radiation and NOAH LSM produced better results. Similar findings were obtained by Jin et al. (2010) who found that land surface processes strongly affected 2-m temperature simulations.

4.1.2 Rainfall

The total rainfall of MRB for the summer (MJJA) of 2009 was simulated by WRF driven by the ERA-Interim reanalysis data of one degree resolution. The results were then compared with the gridded ANUSPLIN rainfall data and also with some observed station data. Some horizontal re-gridding of the dataset of ANUSPLIN was necessary to estimate the bias of rainfall data simulated by WRF over the whole domain of MRB. The results show that for the test category 1 based on a 5–layer Thermal Diffusion Land Surface scheme WRF mainly under-simulated the precipitation of MRB, and only over-simulated the precipitation of the mountainous region of MRB. Details of results (bias) obtained from the 18 sets of experiments for the MJJA 2009 rainfall is presented in figure 23.

The Unified Noah Land Surface Model (Noah LSM) combined with other physics parameters are performed in the test category 2 (tests no. 4 to15), which achieved relatively better agreements with the ANUSPLIN data. Figure 23 shows the bias plots for the test # 11 and 12 for test category 2 (using Noah LSM). For test experiments # 4 to 8 and 13, WRF simulated about 150 mm less precipitation than the ANUSPLIN data for the summer of 2009 even though the results are better than that of the test category one. Results of experiments # 9-12 and 15-16 are better, with an average bias less than 100 mm. Test # 8, 11, 12 were set up with the same physics parameters but different micro-physics options. Micro physics option 3 (WRF Single–moment

3–class Scheme), 16 (WRF Double Moment 6–class Scheme) and 6 (WRF Single–moment 6–class Scheme) were used for test # 8, 11 and 12 respectively.

For the test category 3 using the RUC Land Surface Model, WRF over-simulated the rainfall, with a bias as high as 300 mm over the mountainous region, even though other parts of MRB have negative bias of about 100 mm. Test # 18 suffers more negative rainfall bias across MRB. Test # 16 and 17 use the same Single–moment 3–class microphysics scheme but for the radiation scheme, the CAM Shortwave and Longwave Schemes was used for test # 16, while the Fu–Liou–Gu Shortwave and Longwave Scheme was used for exp. 17.

Through eighteen combinations of microphysics for radiation, land surface and cloud physics of WRF tested, it turns out that test # 11 and 12 agree better with the ANUSPLIN 10 km gridded rainfall data. In terms of the spatial distribution of rainfall pattern, it is clear that WRF has a tendency to simulate more rainfall over the mountainous region but lower rainfall over the northern part of MRB.

To compare the WRF rainfall with the observed rain gauge data, 8 climate stations that represent different parts of MRB are selected. The "Second Generation of Daily Adjusted Precipitation for Canada" was collected from Environment Canada's web site and the data were compared with WRF's simulated rainfall for those grids that correspond to the eight stations.

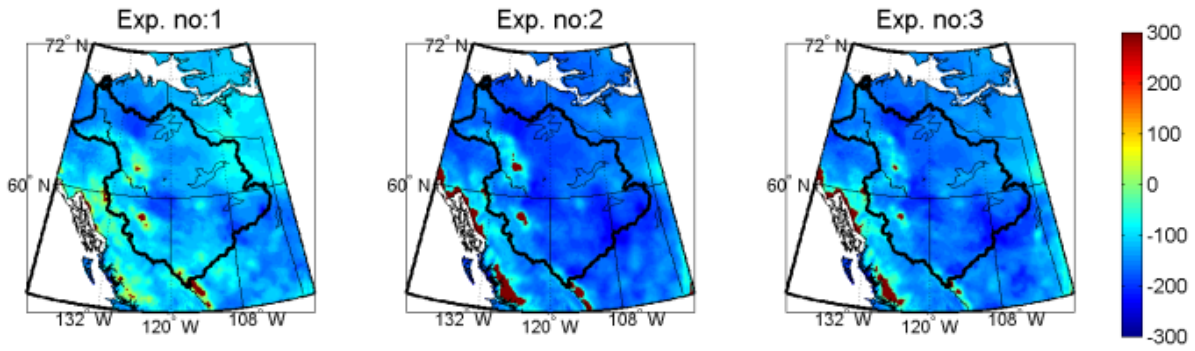

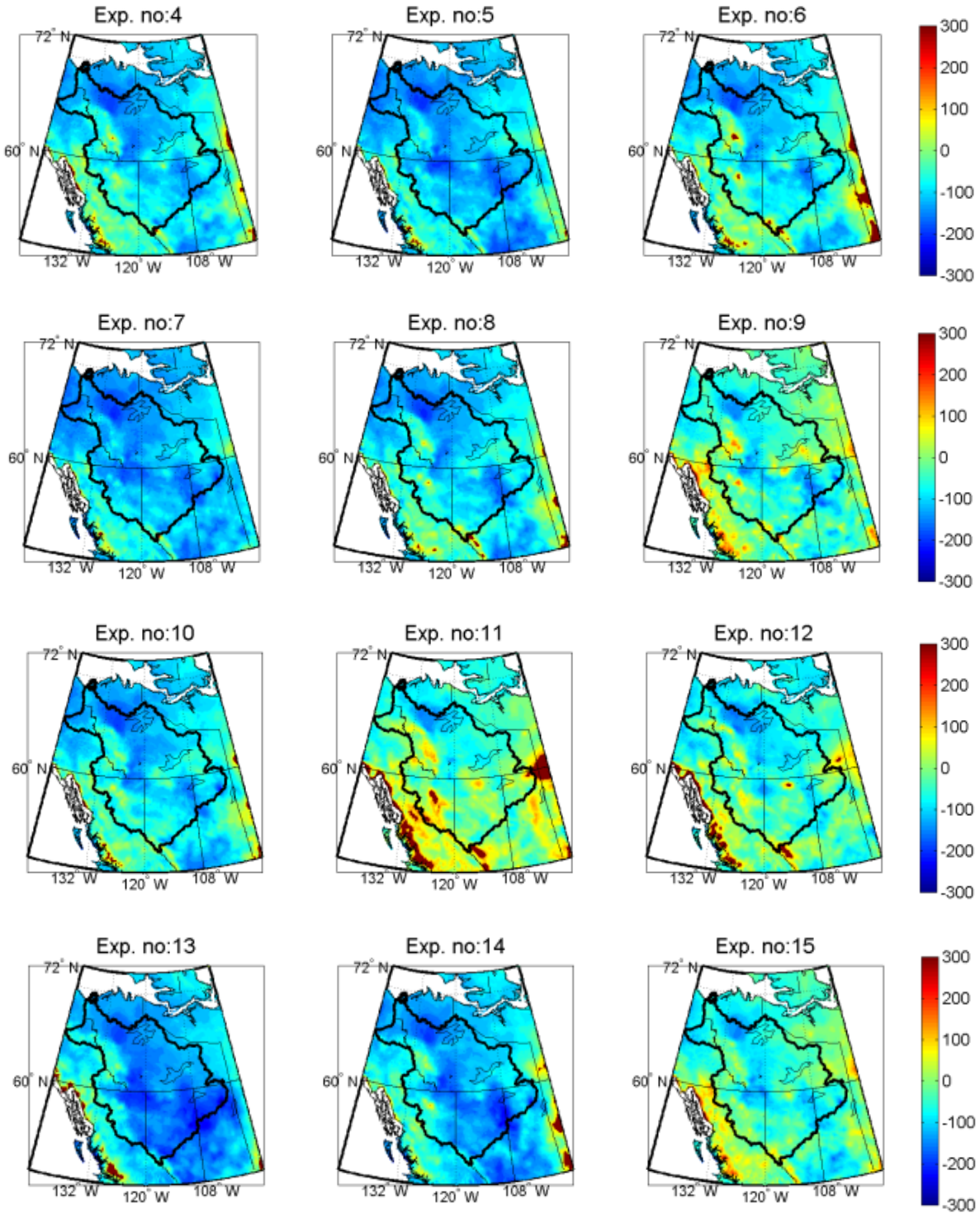
Exp. no:4
Exp. no:5
Exp. no:6
Exp. no:7
Exp. no:8
Exp. no:9
Exp. no:10
Exp. no:11
Exp. no:12
Exp. no:13
Exp. no:14
Exp. no:15
72° N
60° N
132° W
120° W
108° W
300
200
100
0
-100
-200
-300

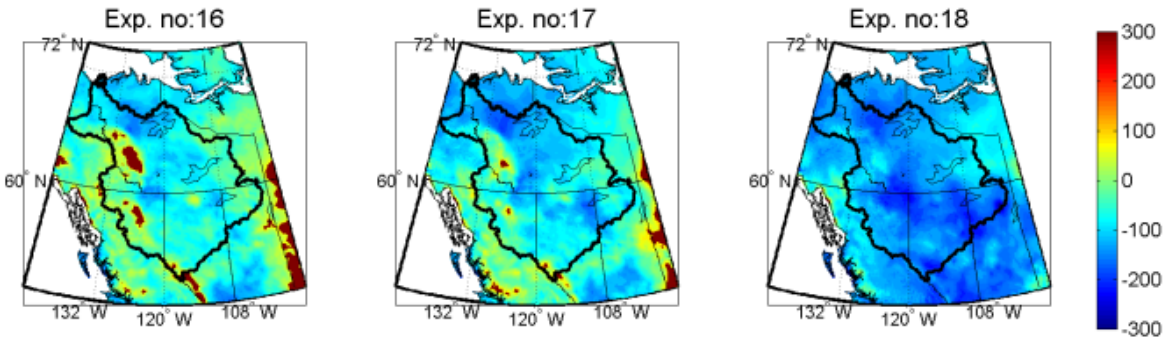

Figure 23**:** Total precipitation bias (WRF-ANUSPLIN) over MJJA of 2009 as the testing period for 18 test cases, test # 1 to test # 18, respectively**.**

Figure 24 shows locations of the selected climate stations over MRB while Figure 25 shows the cumulative rainfall plots for climate station versus WRF's simulations for all three test categories at station 1 (58.8N, -122.6W), station 6 (60.8N, -115.8W) and station 8 (60.1N, -128.8W). Apparently for test # 11, 12 and 16, WRF could simulate comparable precipitation with that of stations 1, 6, 7 and 8, but WRF simulated more precipitation than observed data of stations 2, 3 and 4. However, WRF simulated lower precipitation data than the observed data of station #5 except for experiment # 16.

Figure 24: Location of the selected stations

Among 18 experiments tested with WRF driven by ERA interim reanalysis data, experiment # 11, 12 and 16 agree well with the "Second Generation of Daily Adjusted Precipitation" data for the selected stations and also showed comparable results with respect to ANUSPLIN rainfall data. Plotting of rainfall from the selected stations (station #1, station #6 and station #8), which are representative to central, western and eastern parts of the basin are shown in figure 25.

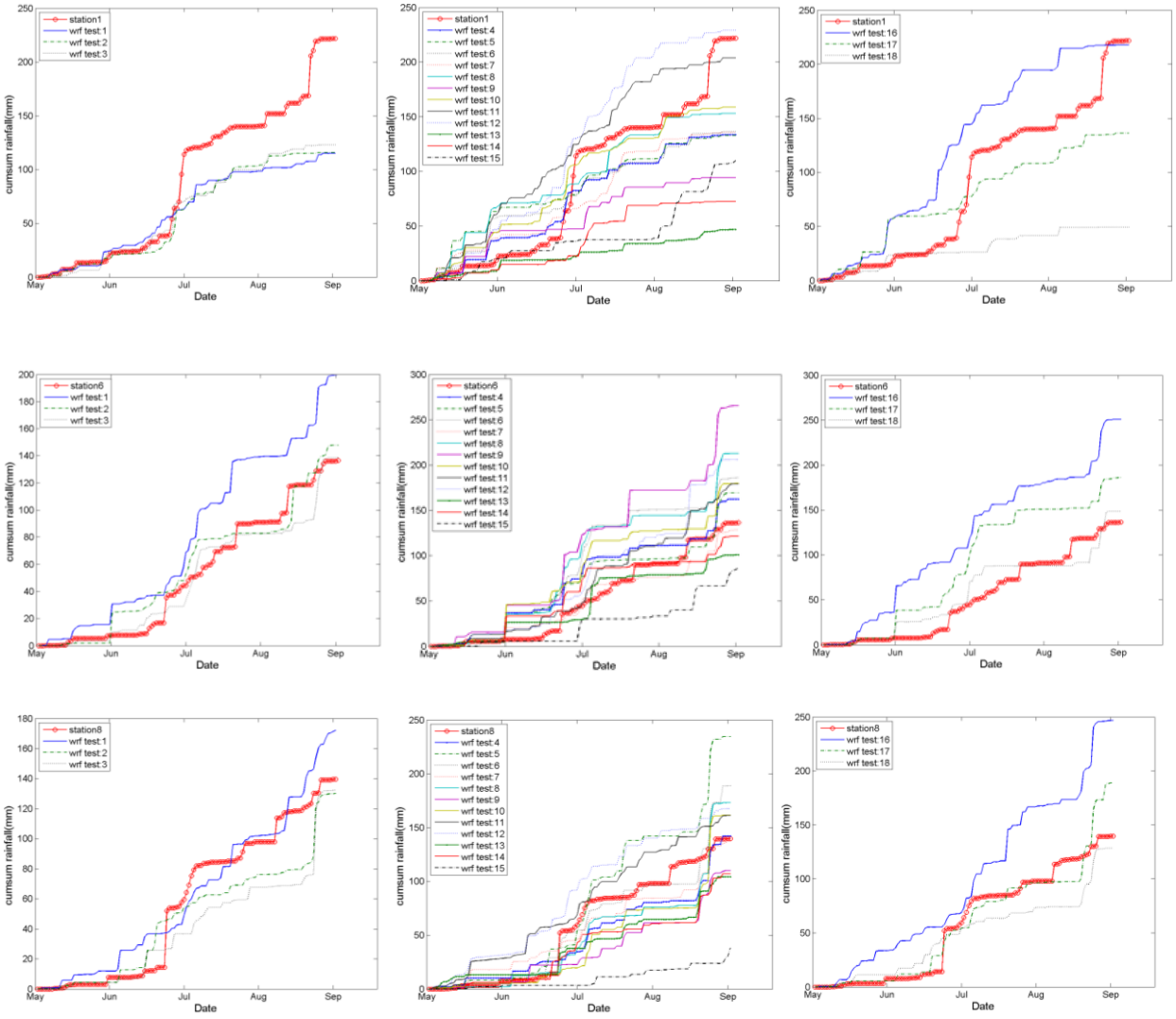

Figure 25: Cumulative rainfall plotting from (a) test category 1 in column 1) (b) test category 2 in column 2 and (c) test category 3 in column 3 are compared with the observed station precipitation data for station 1, 6 and 8 for MJJA, 2009.

The physics options used for experiment # 11 is WRF Double-moment 6–class Scheme for the microphysics, Unified Noah Land Surface Model, CAM shortwave and longwave schemes, Yonsei university scheme (YSU) for the planetary boundary layer physics, and Kain–Fritsch Scheme for the cumulus parameterization. For experiment # 12, the WRF Single–moment 6–class Scheme was used for the microphysics which is the only difference from experiment # 11. For experiment # 16 the same microphysics and the radiation, surface and cloud physics options were selected as experiment no. 12, except that the former used the RUC Land Surface Model and the NCEP Global Forecast System Scheme for the Planetary Boundary Layer (PBL) Physics.

It has been observed that WRF tends to over-simulate rainfall over the western, mountainous side of MRB, but less rainfall over the eastern side of MRB. The same rainfall pattern was also simulated by Szeto et al. (2008b) for MRB. In the summer, cyclonic activities transport lake evaporation towards the mountainous northwest of MRB. Brimelow and Reuter (2008) also found that moisture fluxes from the southern region plays an important role for giving rise to heavy precipitation over the mountainous region, particularly a when low pressure system develops over the basin.

Detailed analysis of rainfall simulated by various WRF setups showed that only several combinations of WRF physics parameters are capable of simulating realistic rainfall over the MRB, particularly test no. 11.

4.2 WRF Validation

Given that test # 11 shows promising results by simulating reliable temperature and rainfall data over MRB for the summer (MJJA) of 2009, it was further tested over multiple years from 1979 to 1991 and validated using the 6-hr, ERA-Interim Reanalysis data. This particular WRF model

setup simulated the climate of MRB at 6 hourly intervals and 30 km x 30 km resolution. The results (temperature and rainfall) were compared with higher resolution (10 km x 10 km) daily ANUSPLIN data. The results of 2 m air temperature are shown in Figure 26. Apparently the selected WRF model setup (test #11) could capture the regional variation of 2m temperature reasonably well. 2 m mean temperature for 1979 to 1991 for the summer (MJJA) shows a reasonable agreement with the ANUSPLIN 2 m temperature data, generally with a 0.5 to1 ^{o}C negative bias over the MRB, but more under-simulation over the mountainous part of MRB.

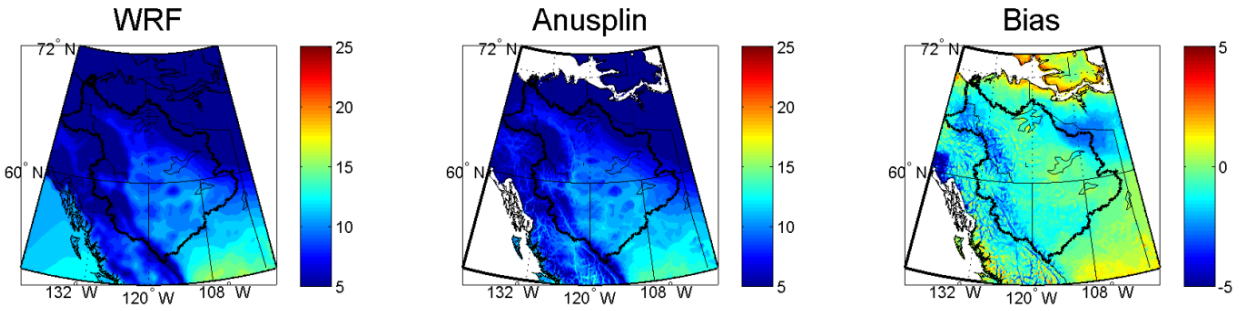

Figure 26: (a) Average 2 m air temperature from WRF output using era data for MJJA of 1979 to 1991 (b) 2 m air temperature from ANUSPLIN data for the same period (c) 2m air temperature bias (WRF-ANUSPLIN).

The ERA-Interim 2 m temperature data compares well with WRF's simulated temperature using the test #11 setup for 1979-1991, with a R^2 of 0.78 (Figure 27). Therefore, the selected WRF setup could simulate the regional temperature of MRB, even though with some obvious bias over the mountains, with similar results obtained by Done et al. (2004) who also found that WRF poorly simulated temperature over the mountains.

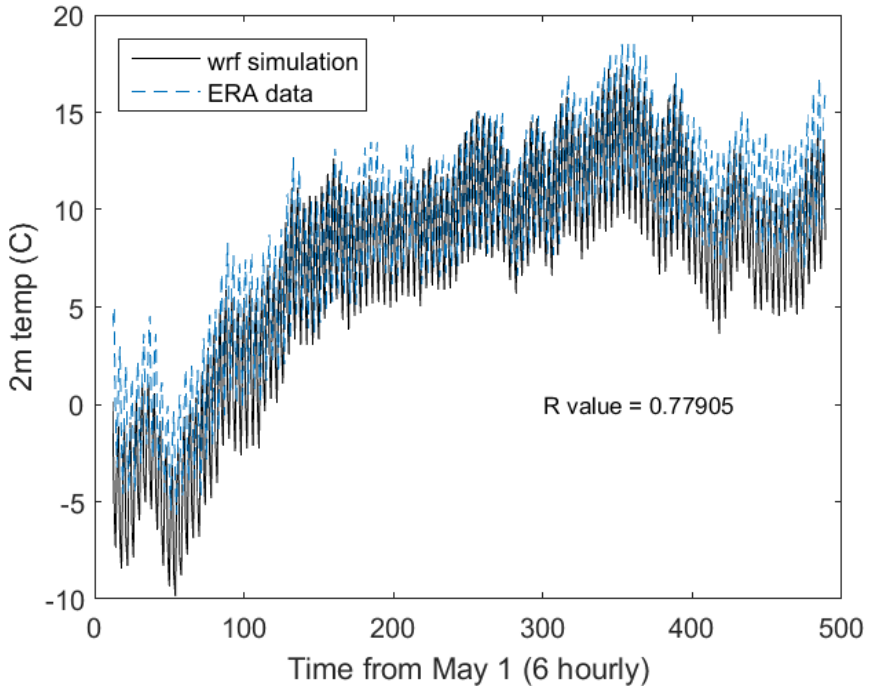

Figure 27: Comparison of WRF outputs from 1979 to 1991 and ERA-Interim 2 m temperature

We also compared the simulated rainfall of WRF test #11 over the validation period of 1979-1991 with the ANUSPLIN data. In general WRF's simulations suffer positive bias compared with the ANUSPLIN daily rainfall data, especially over the mountainous area. In general the Northern part of MRB is very dry and generally gets less than 150 mm rainfall in the summer, while the south has rainfall around 300 mm in the summer, but the western part is even wetter, with an average rainfall exceeding 600 mm. Figure 28 shows that WRF simulated more rainfall (about 200 mm) over the mountaeous area, but simulated rainfall that is comparable ANUSPLIN in the central part of MRB. Apparently WRF has problem simulating realistic rainfall over the complex mountainous terrians of MRB. WRF has been shown to capture the complex interactions between land and lower atmospheric in relatively horizontal terrians, but tends to suffer wither over or under simulation problems over mountaneous terrians (Maussion et al. 2011).

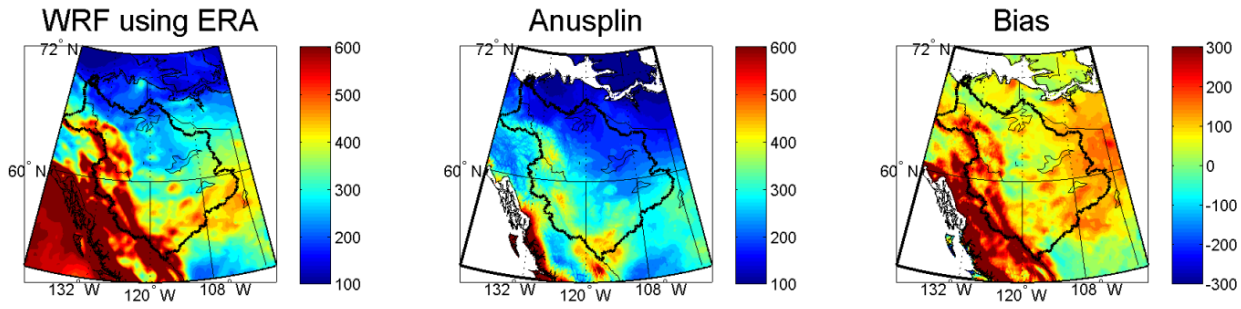

(a) (b) (c)

Figure 28: (a) Average rainfall from WRF output using ERA-Interim data for MJJASO 1979 to 1991 (b) Average rainfall from ANUSPLIN data for the same period (c) Average rainfall bias

4.3 Evaluation of the CanESM2 Historical Data Downscaled by WRF

The 2nd generation Canadian Earth System (CanESM2) couples an atmosphere-ocean general circulation model, a land-vegetation model and terrestrial and oceanic interactive carbon cycle. It simulated the observed 20th's century temperature variability that includes the early and late 20th century warming periods and the intervening 1940–1970 period of substantial cooling reasonably well, but CanESM2 overestimated the post 1970 warming period (Chylek et al. 2011). The CanESM2 raw data of 2.81° x by 2.81° for MJJASO of the historical period of 1979 to 2005 was dynamically downscaled by WRF. The data involved in the downscaling were surface level, pressure level, sea ice, soil moisture and soil temperature data extracted over the area between 25N and 80N, -195 and -45E. The input data for the WRF model were pre-processed at 6 hourly time intervals. The necessary initial and boundary conditions were set up using the WRF Preprocessing System (WPS); the land use data for MRB were taken from the USGS-based land use data set with inland water bodies (usgs_lakes) as the input to the geogrid field.

Using the WRF configuration for test #11, the climate of the Mackenzie River Basin (MRB) were simulated for MJJASO from 1979 to 2005 at 30 km by 30 km resolution and 6 hourly time

steps. The 2-m air temperature data simulated by WRF were compared with the ANUSPLIN 2 m mean temperature. Figure 29 compares WRF's simulated 2 m temperature using the CanESM2 data for MJJASO during 1979 to 2005 with the gridded ANUSPLIN data.

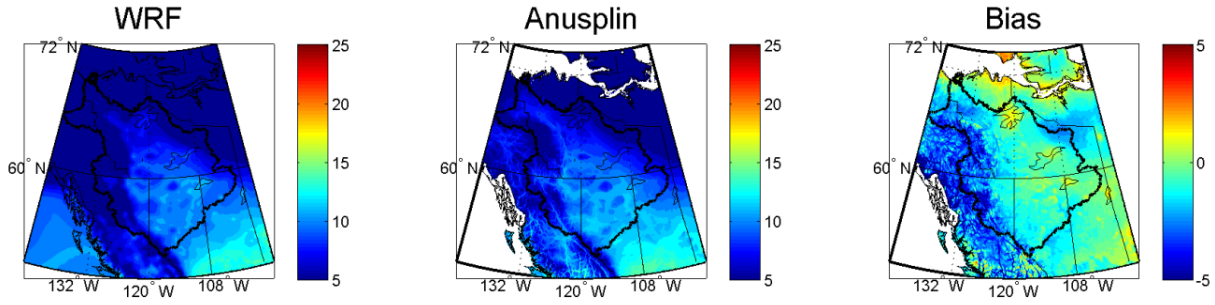

Figure 29: (a) Average 2 m air temperature from WRF output using CanESM2 data for MJJASO of 1979 to 2005 (b) 2 m air temperature from Anusplin data for the same period (c) bias

The results show that WRF could capture the spatial distribution of 2 m air temperature over MRB reasonably well, with about 1 ^{o} C negative bias compared with the ANUSPLIN even though the bias is not evenly distributed across MRB, especially at the Rockies which have more under simulation problems. For the eastern and central part of MRB with relatively flat terrain, the simulated air temperature shows close agreement with the ANUSPLIN data, even though there are some positive or negative bias. As expected, simulating climate processes in a complex, mountainous terrain is more challenging than simulating climate processes in a flat terrain, as similarly reported by Fathalli et al. (2014). Dasari et al. (2014) found significant bias and poor co-relation in air temperature simulated by WRF over complex topographic areas of Europe. A major source of this bias could be due to a lack of representative topography and complex land surface-atmosphere interactions.

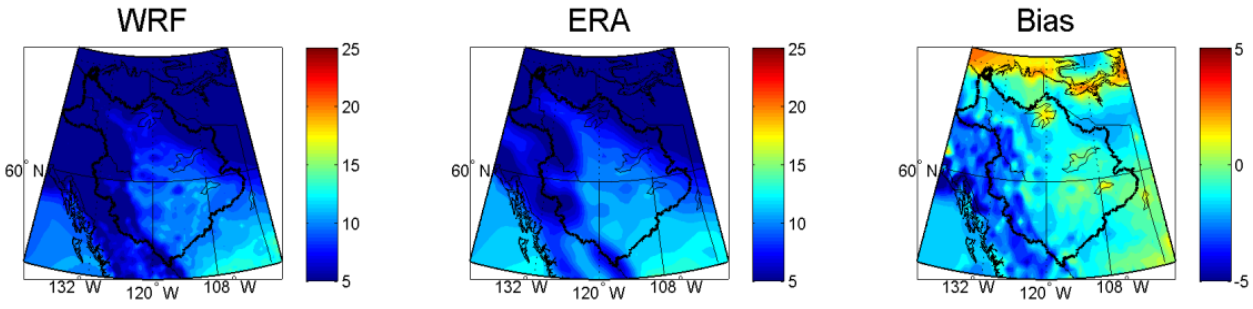

(a) (b) (c)

Figure 30: (a) Average 2 m air temperature from WRF output using CanESM2 data for MJJASO of 1979 to 2005 (b) 2 m air temperature from ERA-Interim data for the same period (c) bias

We also compared the ERA-Interim 2m air temperature with WRF's simulation over the same period. Figure 30 shows that WRF's simulations generally agrees with the ERA-Interim data, but with a negative bias of about 1°C in central and eastern part of MRB, while 2-3 ° C negative bias at the mountainous Rocky areas of MRB. A Scatter plot of these temperature data are shown in Figure 31.The correlation coefficient was 0.81, which indicates a fairly good correlation between WRF's simulations versus the ERA-Interim 2 m air temperature data.

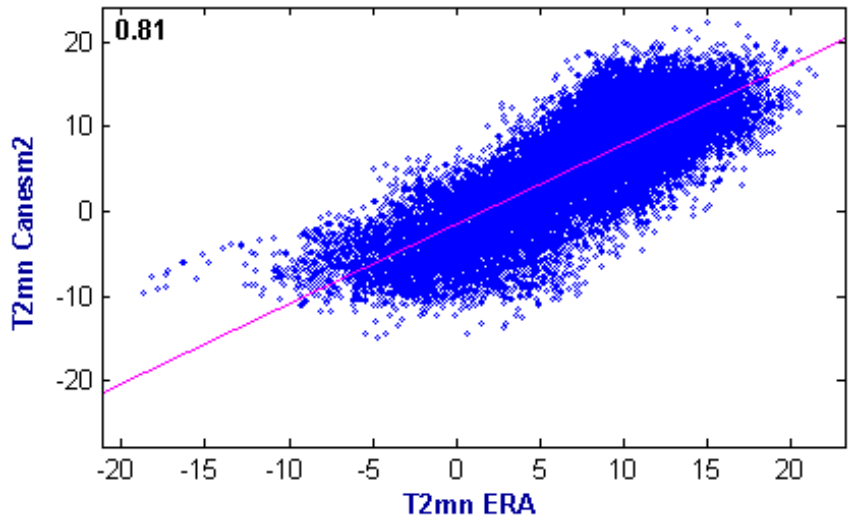

Figure 31: Scatter plot of WRF's simulated temperature from the CanESM2 historical 1979-2005 temperature data and the ERA-Interim 2 m temperature.

To assess WRF's simulated precipitation over MRB for the historical period using CanESM2's historical data and compare with some observed station rainfall data, it seems that WRF could simulate reasonable summer (MJJASO) precipitation pattern over MRB. For example, Edmonton has an average MJJASO precipitation of about 341.3 mm while WRF simulated about 360.5 mm of precipitation. At the Barkerville station (53°04' N 121°30' W), the average MJJASO precipitation has been about 556 mm from the precipitation chart of Canadian Climate Normals (CCN) for 1971 to 2000, while WRF simulated about 540 mm of MJJASO precipitation over 1979- 2005. Similarly for the Hay River station (60°50' **N** 115°46' W), it is 237.2 mm (CCN) versus 255mm (WRF) for MJJJASO; and for the Norman Wells A (65°16' N 126°48' W) it is 205.1 mm (CCN) versus 200 mm (WRF) and for Yellowknife A (62°27' N 114°26' W) it is 194 mm (CCN) versus 200 mm (WRF).

Spatially, most of the mountainous area gets much higher precipitation than the low lying plains of central and eastern parts of MRB, as expected from the moisture circulation pattern of MRB (Brimelow and Reuter 2005), e.g., the observed average MJJASO precipitation over the western mountainous area is about 500-600 mm. It is obvious that WRF over simulates precipitation over the western part of MRB, but it simulates reasonable precipitation over other parts of MRB for the historical period. By comparing with the ANUSPLIN data, it is clear that the bias of WRF's simulation is generally modest over some parts of MRB (Figure 32); but about 250 mm of positive bias in the western part and about 100mm in the north eastern part of MRB when compared with the ANUSPLIN data. Again, it is obvious that WRF has challenge simulating reasonable precipitation patterns over the complex, mountainous terrains of the west.

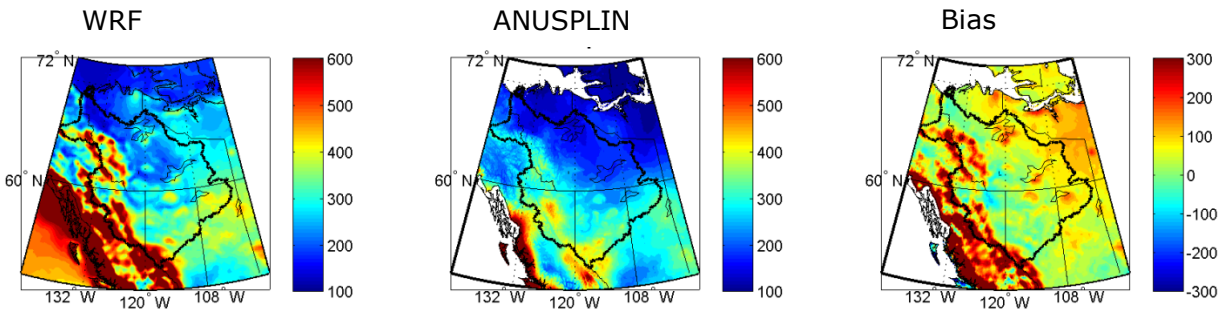

(a) (b) (c)

Figure 32: (a) Average rainfall from WRF output using CanESM2 for MJJASO of 1979 to 2005 (b) Average rainfall from Anusplin data for the same period (c) Average rainfall bias for MJJA of 1979 to 2005

By comparing with the Global Precipitation Climatology Project (GPCP) data the average MJJASO precipitation is about 312.8 mm, while that simulated by WRF is about 331.2 mm rainfall, which shows a modest over-simulation of the summer precipitation by WRF.

On a whole, based on the 2m temperature and precipitation data WRF simulated over MRB for the base period using CanESM2 historical data or ERA-Interim reanalysis data as input, except for the mountainous terrains on the west, it seems that the test #11 setup for WRF is adequate to simulate the regional climate of MRB, even though some bias were observed.

4.4 Future Climate Projections

4.4.1 CanESM2 RCP 4.5 projections for 2050s (2041-2070)

The Canadian Earth System model's (CanESM2) Representative Concentration Pathway (RCP) 4.5 and RCP 8.5 climate change scenarios for 2041-2070 were chosen for projecting the future climate of MRB in the 2050s. The required data were extracted from CCCma (Environment Canada 2003) were pre-processed using the WPS system to provide the initial and the boundary

conditions for WRF. The CanESM2 RCP 4.5 data has a horizontal resolution of 2.81° with 35 vertical layers (Environment Canada 2003). The required variables and vertical levels from CanESM2 RCP 4.5 data were extracted and processed as input to the WRF regional climate model which dynamically downscaled the CanESM2 data to a 30-km horizontal grid resolution, with 28 vertical levels appropriate for regional scale river basins such as MRB. In Figure 33 WRF's downscaled 2-m air temperature from CanESM2 RCP 4.5 2050 (2041 to 2070) data are compared with the historical data. It seems that by 2050s, the northern part of MRB will be 3.0 to 4.0 ^{o}C warmer, while its southeast part will be 2 to 3 ^{o}C warmer. The projected warming by WRF using RCP 4.5 of CanESM2 generally agrees with CMIP5's multi-model ensemble mean projections for summer air temperature. For 2050s, under RCP 4.5, the projected warming is reported to be higher in the north eastern than the southern part of MRB (IPCC 2013).

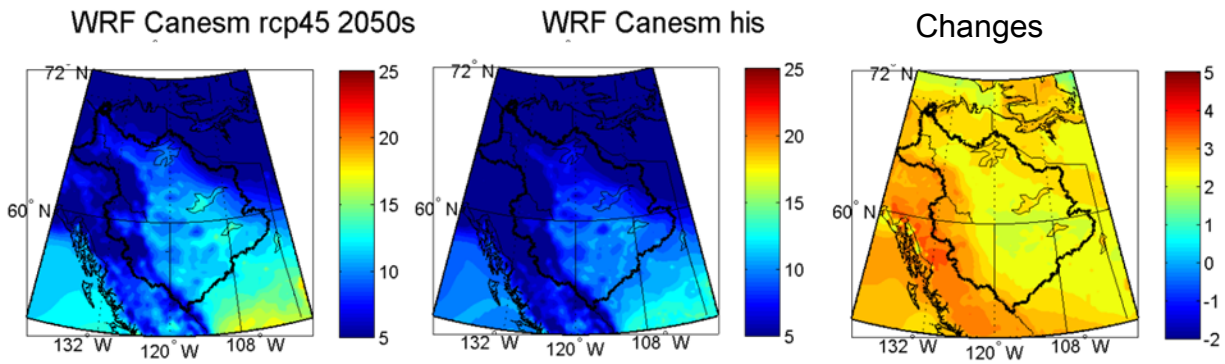

Figure 33: Average MJJASO 2-m air temperature downscaled by WRF using CanESM2 data of (a) 2041 to 2070 and (b) historical period (1979 to 2005).

Figure 34 shows that the projected change of mean surface air temperature of MRB from the downscaled data by WRF model for RCP 4.5 and from the raw GCM CanESM2 data for RCP 4.5 for 2050s. It is observed that the downscaled data essentially captured the distribution of

temperature anomaly over the basin and also the range of temperature changes matches closely with the raw data set.

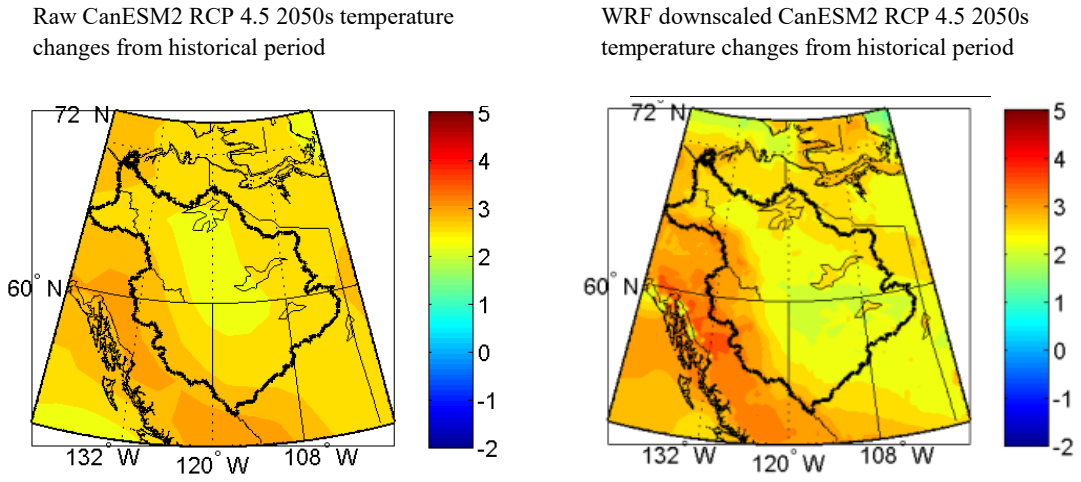

Figure 34: Difference between the raw CanESM2 temperature changes from historical data for RPC 4.5 2050s and that downscaled by WRF.

According to CanESM2's RCP 4.5 climate scenarios downscaled by WRF, on an average MRB and Canada is expected to become wetter in the 2050s compared to historical period of 1979-2005, even though some parts of MRB, especially the Eastern part, may not experience wetter climate in the 2050s. Figure 35 shows the MJJASO precipitation of MRB that WRF downscaled from CanESM2 historical (1979-2005) and RCP 4.5 data for 2041-2070, and their difference. The projected change in the MJJASO precipitation over the basin is mostly positive and with an average change of 75 mm, but the Rockies on the west is projected to increase by 150 mm in 2050s relative to the base period. The projected change in the Northern part of MRB is relatively modest between the base period and 2050s under RCP 4.5 climate scenario. The projected increase in precipitation by the 2050s is expected, given the atmosphere can accommodate more water vapor under a warmer climate.

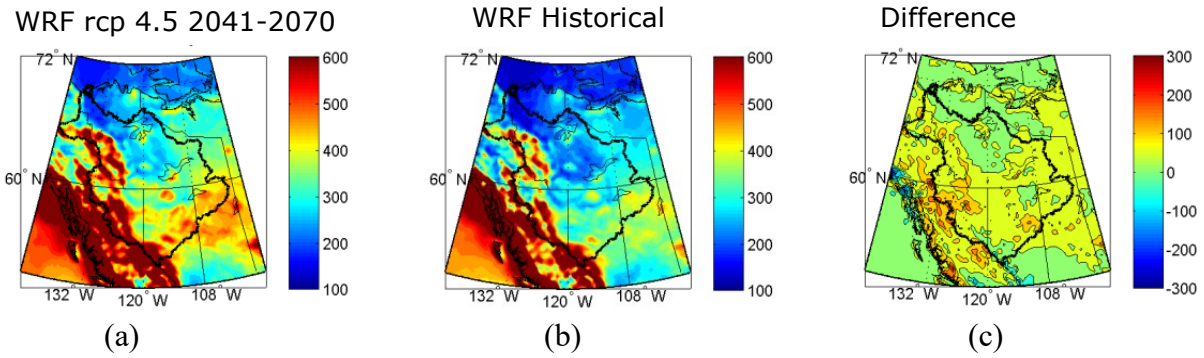

Figure 35: Rainfall that WRF downscaled from CanESM2 data for RCP 4.5 over (a) 2041-2070 and (b) the base period of 1979 to 2005 (c) Changes in 2050s

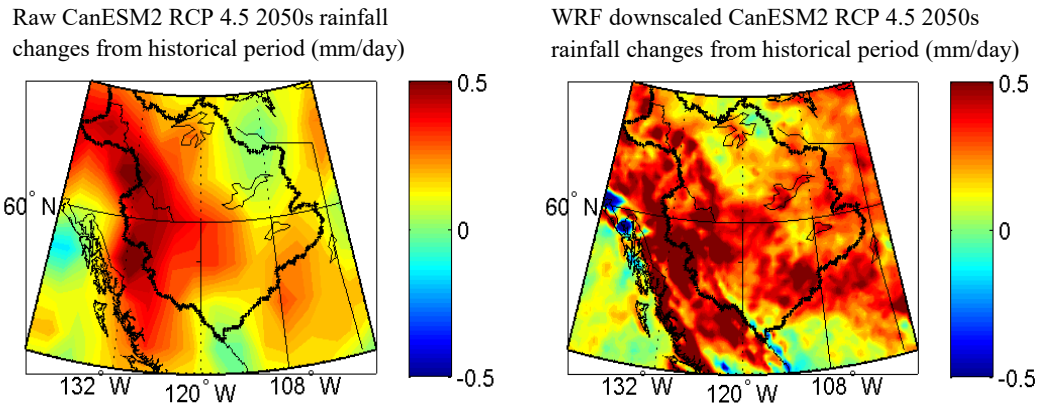

Figure 36: Difference between the raw CanESM2 precipitations changes from historical data for RPC 4.5 2050s and that downscaled by WRF.

We also compare the GPCP precipitation data with that downscaled by WRF for the historical period, and for the 2050s. According to CanESM2 RCP 4.5, the precipitation of MRB is projected to increase by about 75 mm for MJJASO. WRF marginally estimated more precipitation than the GPCP precipitation data over the base period. Figure 36 compares the WRF downscaled and raw Canesm2 RCP 4.5 precipitation data for MRB.

On a whole, based on the projection of CanESM2 RCP 4.5 climate scenario, MRB is projected to become warmer and wetter by 2050s compared to the base period of 1979-2005. Warming is expected to be more pronounced in the Rockies of the western part of MRB and also in the north

than in the central, eastern and southern plains of MRB. As expected, the projected changes in temperature and precipitation will likely not be evenly distributed across the river basin, especially precipitation. In other words, some parts of MRB will likely experience more pronounced change than others.

4.4.2 CanESM2 RCP 8.5 simulations for 2050s (2041-2070)

The RCP 8.5 climate scenarios assume high greenhouse gas concentrations in 2100 (IPCC 2013). Radiative forcing in RCP4.5 peaks at about 4.5 W/m^2 (~540 ppm CO2) while RCP8.5 assumes a high rate of radiative forcing increase, peaking at 8.5 W/m^2 (~940 ppm CO2) in year 2100. Therefore RCP8.5 assumes higher CO_2 concentrations than the SRES A2 scenarios by 2100. The CanESM2 RCP 8.5 climate scenarios of 2050s that project the temperature of North America to increase by 3-5 ^oC were downscaled by WRF.

The MJJASO 2-m air temperature that WRF downscaled from CanESM2 RCP 8.5 data for 2041 to 2070 at 30 km by 30 km resolution shows that air temperature in the 2050s can be between 2 and 5 ^oC higher than the historical period (Figure 37). More modest warming of about 2-3 ^oC is projected for the central region and higher projections (3 to 5 ^oC) for the western and north-eastern part of MRB. Figure 38 shows that the projected change of mean surface air temperature of MRB from the downscaled data by WRF model for RCP 8.5 and from the raw GCM CanESM2 data for RCP 8.5 for 2050s. It is observed that the downscaled temperature change has essentially captured the distribution of temperature anomaly over the basin and also the range of temperature changes matches closely with the raw data set.

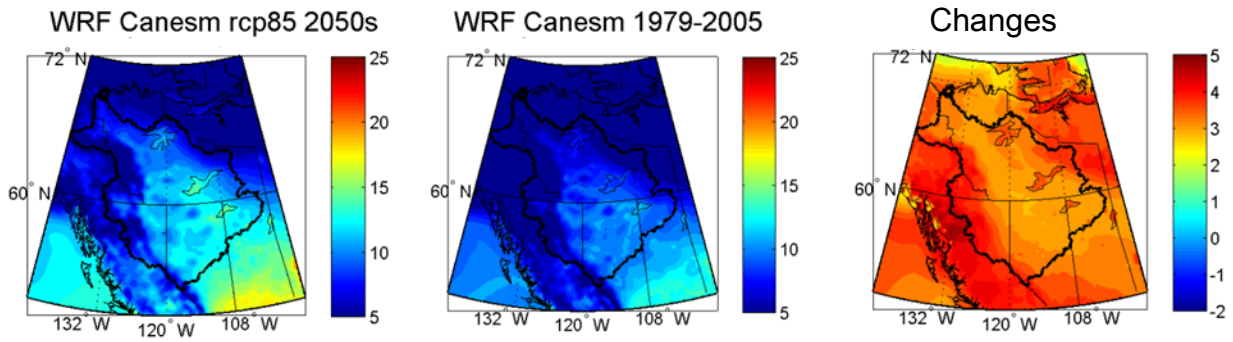

(a) (b) (c)

Figure 37: The MJJASO 2-m air temperature that WRF downscaled from CanESM2 RCP 8.5 data for (a) 2041 to 2070, for (b) historical period, 1979 to 2005, and (c) the difference.

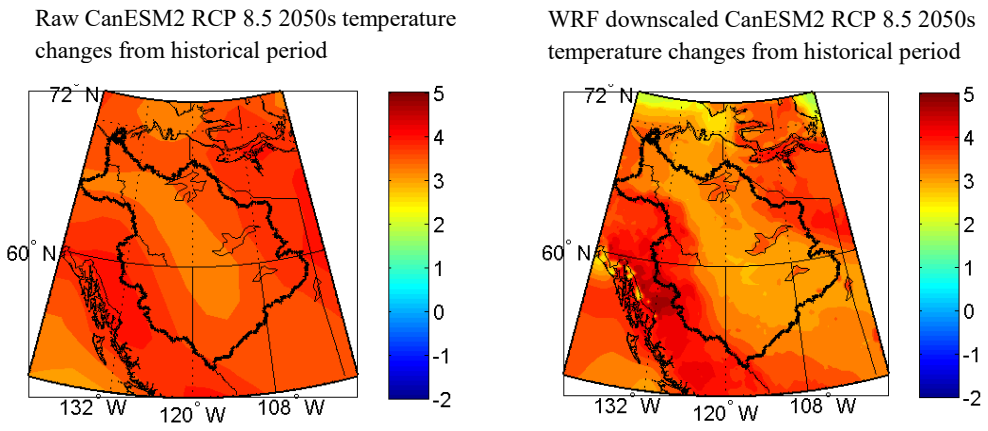

Figure 38: Difference between the raw CanESM2 temperature changes from historical data for RPC 8.5 2050s and that downscaled by WRF.

The MJJASO precipitation that WRF downscaled from CanESM2 RCP 8.5 data for MRB from 2041 to 2070 mostly shows positive change over the historical period, which ranges from 50 mm to 150 mm, and average about 85 mm (Figure 39). As expected, the RCP 8.5 scenario of CanESM2 projects a stronger positive change in precipitation of MRB than the RCP 4.5 counterpart. Figure 40 shows that the projected change of rainfall of MRB from the downscaled

data by WRF model for RCP 8.5 and from the raw GCM CanESM2 data for RCP 8.5 for 2050s from the historical period.

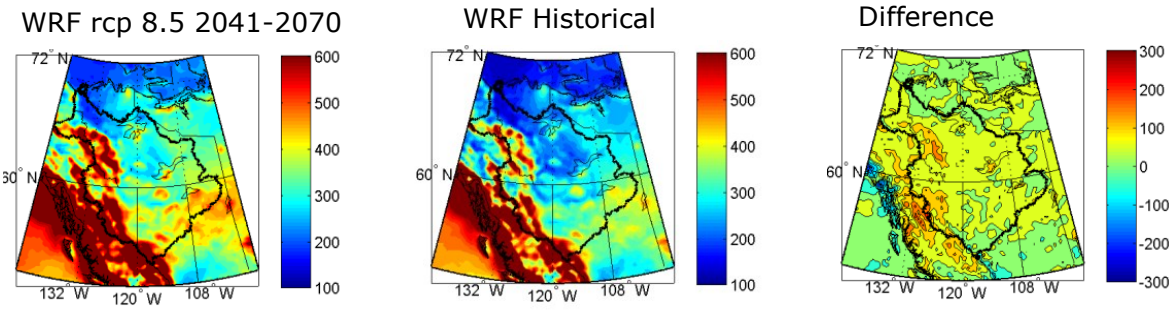

Figure 39: The MJJASO precipitation that WRF downscaled from CanESM2 RCP 8.5 climate scenario for (a) 2041 to 2070, for (b) the historical period of 1979 to 2005, and (c) the difference.

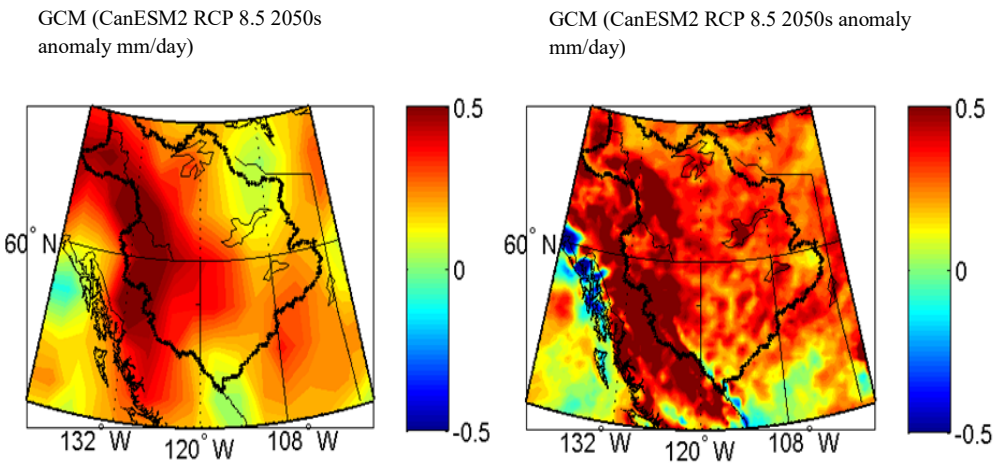

Figure 40: WRF simulated rainfall rate and GCM (raw Canesm2 RCP 8.5) rainfall rate anomalies for RCP 8.5 2050s

4.4.3 Difference between RCP 4.5 and RCP 8.5 climate scenarios

The CanESM2 climate scenarios downscaled by WRF for RCP 8.5 projects warmer and wetter climate than RCP 4.5 for MRB in 2050s. We will expect different GCMs to project different RCP climate scenarios for MRB. The projected and historical temperature data for MRB by ERA-Interim, ANUSPLIN, and CanESM2 are shown in Table 4. With respect to the historical temperature data of CanESM2, depending on the type of temperature, the average projected

warming of RCP 4.5 exceeds 2 ^{o}C while that of RCP 8.5 exceeds 3 ^{o}C for MRB in MJJASO. However, the mean temperature of the Era-Interim and ANUSPLIN data for the historical period are about one ^{o}C higher than that of the CanESM2 historical data.

Table 5: Statistical comparison of 2m air temperature data:

Statistics	ERA-Interim 1979-2005	ANUSPLIN 1979-2005	CanESM2 Historical	RCP4.5 2050s	RCP8.5 2050s
min	-18.6	-8.9	-12.5	-9.5	-8.5
max	21.4	18.8	27.2	32.1	32.9
mean	6.8	6.3	5.6	8.2	8.9
std	5.9	4.9	4.4	6.9	7.9
q25	2.6	2.2	1.1	2.9	3.9
q50	6.6	6.0	5.7	8.3	8.5
q75	11.3	10.5	11.7	14.6	15.4
q95	15.3	13.2	17.1	20.9	21.9
kurt	2.6	2.0	2.3	2.5	2.5
skew	-0.44	-0.31	0.11	0.34	0.31

The MJJASO precipitation data that WRF downscaled from CanESM2 data for the historical period (1979-2005), RCP 4.5 and RCP 8.5 climate scenarios are compared with the GPCP precipitation data for the historical period to investigate the projected changes in precipitation for MRB in 2050s. Figure 41 shows boxplots of precipitation WRF downscaled from CanESM2 data for the base period (1979-2005), RCP 4.5 and RCP 8.5 for 2050s. According to the boxplots, the projected change in the mean total precipitation of MRB for MJJASO from the historical period will be about 75 mm for RCP 4.5 and about 85 mm for RCP 8.5 climate scenarios, respectively.

This implies that on an average the MJJASO precipitation is expected to increase by about 20-40% for RCP 4.5 and about 20-50% for RCP 8.5 over the central and western part of MRB by 2050s. This means that based on downscaled RCP4.5 and RCP 8.5 climate scenarios, a wetter and warmer climate is projected for MRB in 2050s.

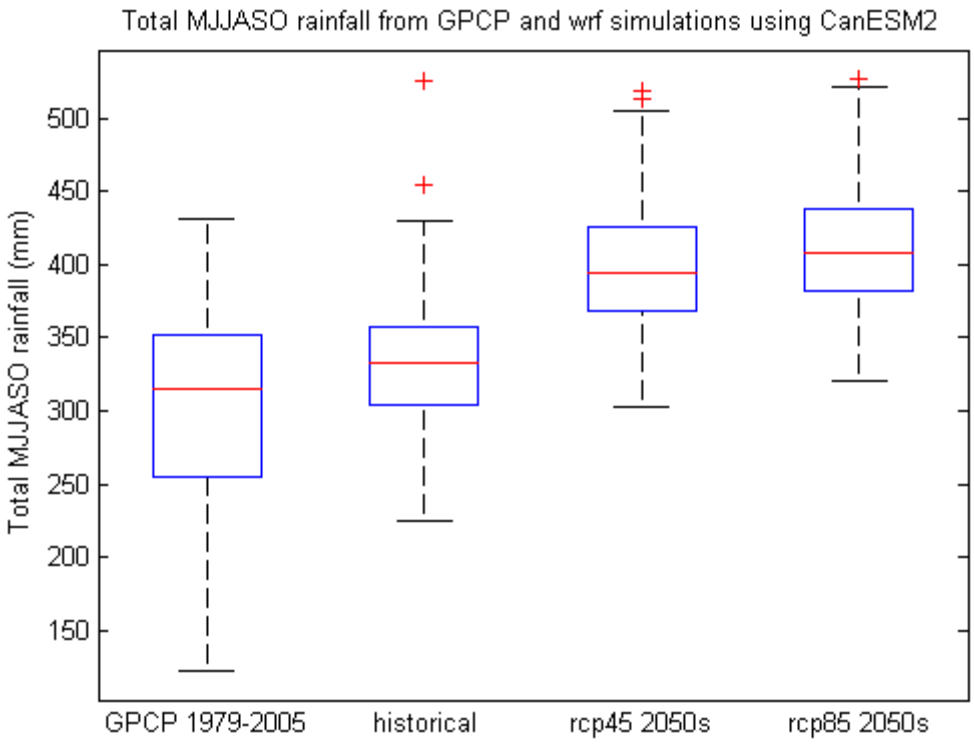

Figure 41: Box plots of historical and projected total MJJASO precipitation compared with the GPCP precipitation data.

On the basis that MJJASO temperature and precipitation patterns that WRF downscaled from ERA-Interim reanalysis data and from the CanESM2 historical data generally compares well with the ANUSPLIN and GCPC data, it seems that as a regional climate model, WRF can generally simulate credible regional climate of a very large and complex Mackenzie River Basin after it is carefully fine-tuned and tested. However, as expected, it will be more challenging to simulate the climate of a mountainous basin such as the Canadian Rockies located on the west

side of the river basin, partly because of a lack of high resolution, DEM data for the Canadian Rockies and partly because even with a domain setup of 30 km x 30 km resolution, it is likely too coarse to model the micro-physics and the local climate of a rugged, mountainous terrain.

4.5 Stream Flow Simulation

The WRF model output, 2m air temperature and precipitation data were used to input to the HBV hydrological model to simulate the stream flow of MRB to the selected stations. This study is kept limited to RCP 4.5 2050s steam flow simulation.

4.5.1 Calibration and validation of the HBV model

HBV was calibrated against streamflow of seven river gauging sites separately, starting first from sub-basin #1, then sub-basin #2, until sub-basin #7, on the basis of simulated streamflow verses observed streamflow for each individual sub-basin. This resulted in seven sets of optimized HBV parameters for the seven sub-basins of the MRB. Streamflow on the Peace River have been regulated after the W.A.C. Bennet Dam was built. Naturalized streamflow for stations 07HA001 and 07KC001 were obtained from the Government of Alberta. An upstream portion of the Athabasca River basin was modelled at station 07BE001. Station 07NB001 on the Slave River included the flow from Athabasca River and Peace River. The Liard river streamflow was modelled at station 10ED002 which, in addition to the outflow from the Great Slave Lake, contributed to the streamflow at Fort Simpson at station 10GC001. The Fort Simpson station was the most upstream site where observed streamflow of the Mackenzie River was used for calibration. The HBV model is not suitable to model the hydrology of the Mackenzie Delta because it is a wetland. Therefore the most downstream station selected for the Mackenzie River was the Arctic Red River at station 10LC014. Based on the availability of

observed input data (streamflow, precipitation and temperature) the calibration period was selected as 1 January 1974 to 31 October 1997 and the validation period from 1 April 1998 to 31 December 2004. The first year (1 January 1973 to 31 December 1973) data was used as spin-up in HBV and therefore was not included in the analysis.

The HBV model was automatically calibrated using streamflow data from 1/1/1974 – 31/10/1997 for each of the seven selected sub basins separately. However, only results for the Fort Simpson (10GC001) and Arctic Red River (10LC014) stations are discussed below. Both climate station data and ANUSPLIN data was used in the calibration, which yielded different optimized parameters as ANUSPLIN is gridded data and not adjusted for changes in elevation. The coefficient of determination and the NS coefficient for the Fort Simpson station based on climate station data are 0.86 and 0.82 for the calibration period, respectively. The corresponding statistics using ANUSPLIN as the calibration data was marginally better, 0.89 and 0.88 respectively. The R^2 and NS for the validation runs at Fort Simpson using the climate station (ANUSPLIN) data was 0.85 (0.85) and 0.77 (0.81), respectively. At the Arctic Red River station, the climate station data had goodness-of-fit statistics ranging between 0.74 and 0.77 for the calibration and validation runs. The ANUSPLIN data resulted in a R^2 and NS of 0.89 for the calibration run, and an R^2 of 0.87 and NS of 0.80 in the validation run, respectively.

Given HBV's simulated streamflow driven by both the climate station and ANUSPLIN input data generally matches well with the observed flow at the validation stage, this means that HBV is well calibrated, its optimized model parameters are physically meaningful, and therefore it can be used to simulate the impact of climate change to the Mackenzie River. HBV accurately simulated the spring snowmelt which has a sharp peak compared to the winter flow, but it

marginally under-simulated the falling limb of the hydrograph. The simulated base flow in the winter is under-simulated compared to the observed flow. This is expected as the observed flow includes the effect of regulated streamflow which have higher winter releases.

4.5.2 Projected changes to streamflow Regimes

After the HBV model was calibrated and validated with the HYDAT streamflow data of Environment Canada, WRF outputs (rainfall and temperature) were forced with HBV to simulate the future streamflow of MRB. Since WRF over simulates of the precipitation and slightly under simulate the temperature over MRB, quantile-quantile bias correction method was applied to the WRF downscaled CanESM2 data with respect to the ANUSPLIN data, before it is being used to drive the HBV model.

The streamflow hydrographs of MRB simulated using the WRF downscaled CanESM2 historical data were compared with the observed historical streamflow at the Fort Simpson station and at Arctic Red River Station; they were further compared with the simulated streamflow using PCIC data for the historical period at the same locations. Figure 42 (a) and (b) show that, the streamflow simulation using the WRF downscaled CanESM2 historical data are comparable with the observed streamflow, as well as with the PCIC historical streamflow for the both Fort Simpson and Arctic Red River stations. Figure 42 (a) and (b) are presented at weekly time scale averaged over the historical period in terms of water levels of the Mackenzie River.

Then, the future water levels at the selected stations were simulated using HBV model; the future climate scenarios RCP 4.5 and RCP 8.5 of CanESM2 data downscaled by WRF were input to derive the streamflow hydrographs of MRB for the 2050s. Figure 43 (a) and (b) show the future water levels in 2050s of CanESM2 RCP 4.5 and PCIC 2050s at Fort Simpson and Arctic Red

River station; in comparison with the observed historical water levels, it is projected that the water levels at 2050s over the MJJASO period will be significantly decreasing at Fort Simpson station; whereas the Arctic Red River will be experiencing reducing of peak flow by 2050s.

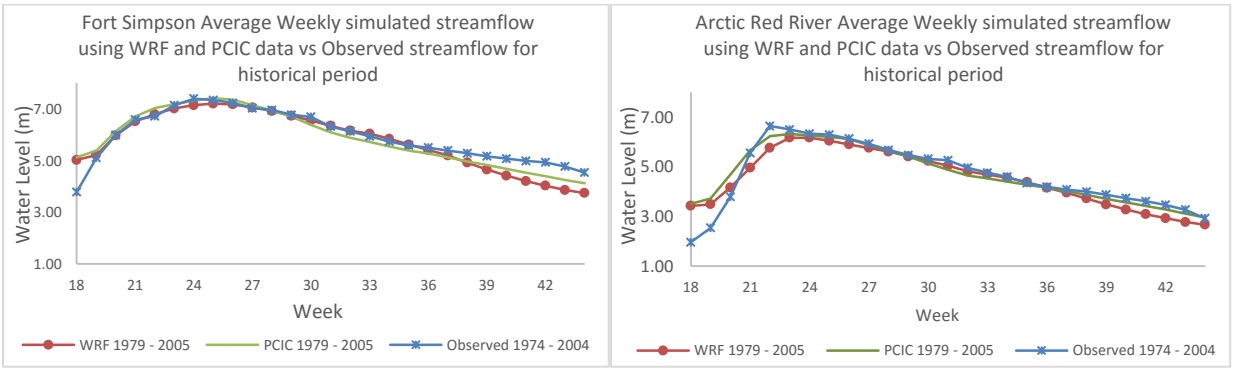

Figure 42: Simulated daily water levels at the Fort Simpson Station using WRF downscaled CanESM2 historical data, PCIC historical data, compared with the observed historical water levels at (a) Fort Simpson station (b) at Arctic Red River station.

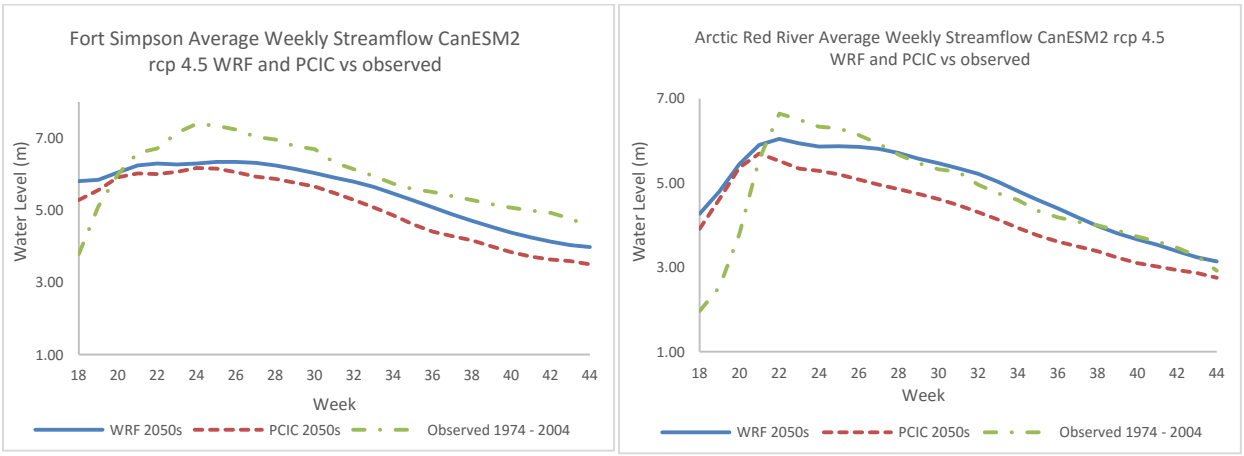

Figure 43: Projected water levels at Fort Simpson Station using WRF downscaled CanESM2 RCP 4.5 2050s, PCIC 2050s, compared with the observed historical water levels at (a) Fort Simpson station (b) Arctic Red River station.

Seasonal (MJJASO) streamflow hydrographs of MRB simulated for the 2050s expressed in terms of water levels of the Mackenzie River for RCP 8.5 are presented in Figures 44 (a) and (b) at weekly time scale averaged over a 30-year periods for the Fort Simpson and the Arctic Red River stations, respectively. The corresponding observed water levels over 1974-2004 is also plotted to demonstrate the projected changes to the streamflow and water levels of the Mackenzie at the Fort Simpson River and the Arctic Red River stations in the 2050s for RCP 8.5 climate scenarios. Substantial lowering of water levels at the Fort Simpson station are projected by 2050s using WRF downscaled CanESM2 RCP 8.5 data; whereas the Arctic Red River will be experiencing reduced peak flow which are also projected to shift about two weeks earlier than the historical peak flow.

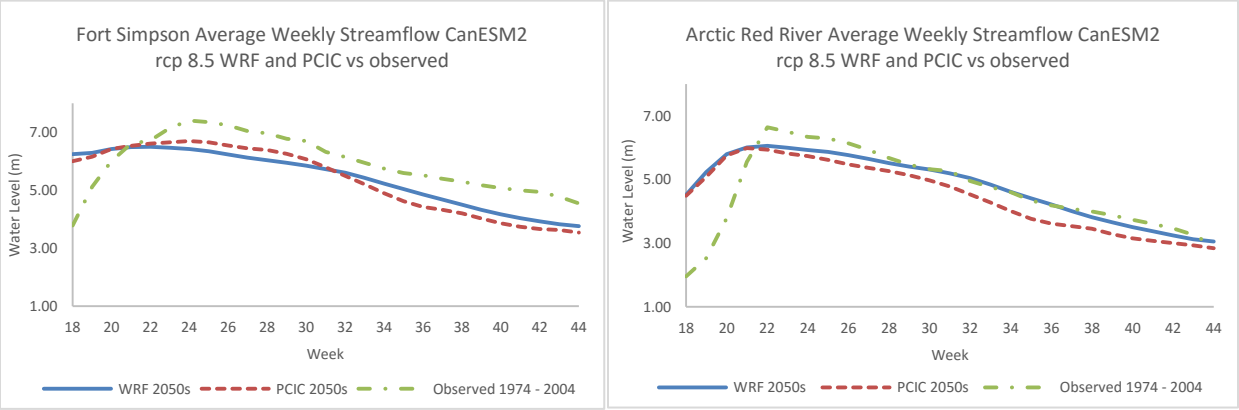

Figure 44: Projected water levels at the Fort Simpson Station using WRF downscaled CanESM2 RCP 8.5 2050s, PCIC 2050s, compared with the observed historical water levels (a) Fort Simpson station (b) at Arctic Red River station.

Since the Fort Simpson station shows significant change in the future water levels, we use the boxplots to statistically compare the results. Figure 45 the boxplots represents the average weekly water levels of MJJASO for each time period (historical and 2050s for RCP 4.5 and RCP 8.5). The observed historical mean water level at Fort Simpson station matches with the WRF

downscaled CanESM2 data derived HBV simulated mean historical water levels. In 2050s the mean water level will be lowering by 300 cm with respect to historical period, on the other hand the peak flow and the high water events will be lowering significantly for both RCP 4.5 and RCP 8.5.

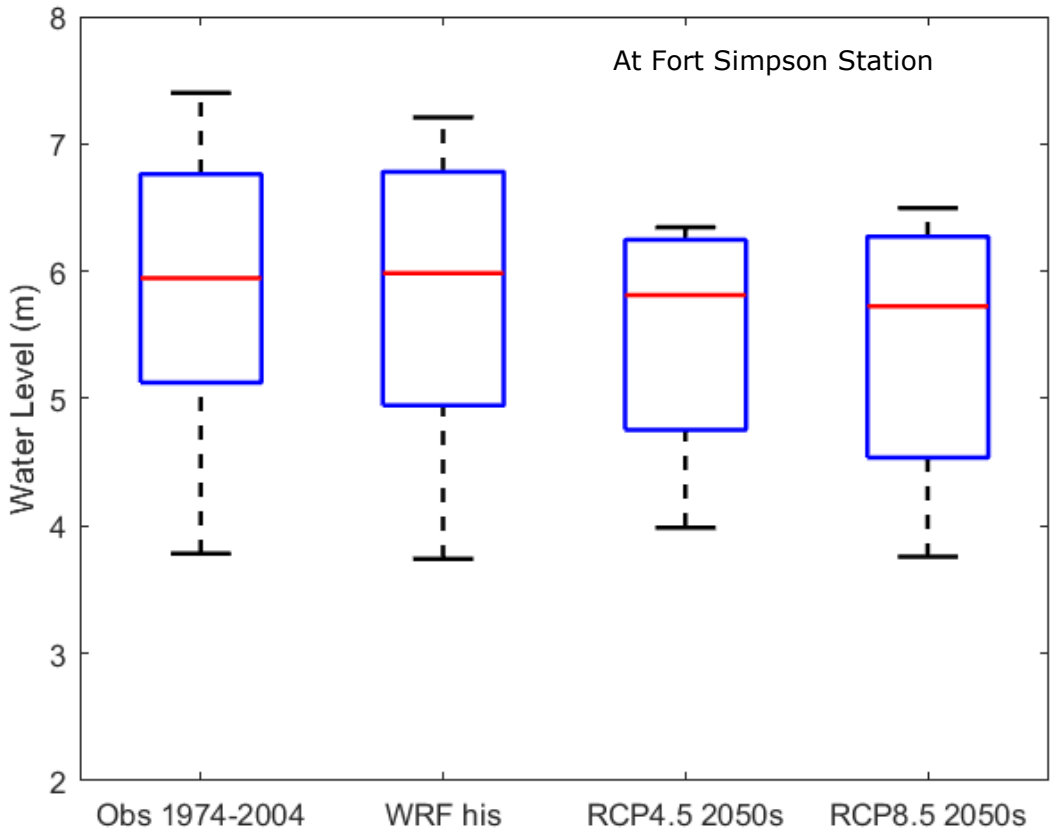

Figure 45: Boxplots of weekly water levels at the Fort Simpson Station using WRF downscaled CanESM2 historical, RCP 4.5 2050s, RCP 8.5 2050s and the observed water levels.

Under a warmer climate, more evaporation loss is expected in the summer; this increase of evaporation could offset the projected increase in precipitation, giving rise to an overall decrease in streamflow and lower water levels in 2050s. The projected lower streamflow and water levels could significantly affect the future hydrology and thus the navigability of the Mackenzie River which is the backbone of water transportation in the western portion of the Northwest Territories.

Navigation problems of the Mackenzie River include a short shipping season (beginning of June to mid-October) and lower water levels. Given the summer water levels of the Mackenzie are projected to decrease in the 2050s, navigation problems related to low water levels are expected to increase in future because safe transit through the Mackenzie River depends on its water levels.

CHAPTER 5

SUMMARY AND CONCLUSIONS

In this study, the regional climate model, WRF, was systematically tested to obtain the optimal configurations to accurately simulate the regional climate of Mackenzie River Basin (MRB). The model settings of WRF (e.g., shortwave radiation scheme, longwave radiation scheme, and MP parameterization schemes), the model performance and sensitivity were investigated. In addition to precipitation and temperature, WRF was also assessed in terms of other climate variables: incoming shortwave and longwave radiations, perceptible water, and albedo, as an effort to identify a model setting that can comprehensively and reliably simulate the regional climate of MRB.

Several long-term simulations (baseline and projected periods) had been conducted. First, the long-term simulations (1979-1991) based on ERA-Interim reanalysis data were completed for validating the performance of the WRF configuration. Next, WRF simulated the climate of MRB for the base (1979-2005) and projected periods (2041-2070) under RCP4.5 climate scenarios of the CanESM2 GCM of Canada.

Based on the RCP 4.5 climate scenarios of the CanESM2 GCM downscaled by WRF, air temperature is projected to consistently increase to about 3 ºC within the MRB in the 2050s, compared to the baseline (1979-2005) air temperature of MRB. Generally, climate change is projected to impact the air temperature marginally higher in colder regions of higher latitude and elevation, such the Canadian Rockies on the western part of MRB.

Based on WRF's downscaled RCP4.5 climate scenarios of CanESM2 GCM, precipitation is projected to increase in MRB, to about 20-40% in the 2050s. In terms of spatial patterns, precipitation can increase up to 30% in northern MRB and the Canadian Rocky Mountains, but only marginal changes are projected in other parts of the MRB.

Analysis of WRF's downscaled temperature from the CanESM2 GCM data for the historical period generally shows a good agreement with the ANUSPLIN data. However, temperature in the Canadian Rockies is mostly under-simulated. WRF's downscaled precipitation from the CanESM2 GCM data also agrees with the ANUSPLIN precipitation data, even though positive bias is detected in the Canadian Rockies. Under downscaled RCP 4.5 climate scenarios of CanESM2 GCM, the 2-m air temperature is projected to increase by 2 to 4 ºC in the MJJASO season in the 2050s. Spatially, the western part of MRB is projected to experience higher temperature rise than the central part.

Under WRF's downscaled RCP 8.5 climate scenarios of CanESM2 GCM, temperature and precipitation of MRB are projected to increase in the 2050s. The 2-m air temperature could increase to 2-5 °C. Warming is projected to be more pronounced in the Canadian Rocky, to about 4- 5 ºC, whereas the central part of MRB could experience 2-3 ºC increase in temperature. On an average, about 85 mm increase in precipitation is projected by RCP 8.5 climate scenarios of CanESM2 downscaled by WRF in the 2050s. Apparently this agrees with an increasing precipitation trend of about 75mm for MJJASO of the baseline period.

Next, the HBV model (hydrological model) of Sweden was calibrated and validated for seven sub-basins located in the MRB using the streamflow data of HYDAT of Environment Canada and both climate station data and ANUSPLIN gridded precipitation and air temperature data.

HBV calibrated using the gridded ANUSPLIN data was selected to model future streamflow as the available downscaled RCP climate change scenarios are also in gridded format. The calibrated HBV driven by the ANUSPLIN data achieved a R2 of 0.85 – 0.87 at the validation stage independent of the calibration experience. Given the calibrated HBV model performed well at the validation stage, there is basis to use the calibrated HBV to simulate the future streamflow and the water levels of the Mackenzie subjected to the potential impact of climate change represented by WRF downscaled climate projections for RCP 4.5 climate change scenarios for the 2050s.

Under the projected increase in air temperature and precipitation of RCP 4.5 climate change scenarios of the CanESM2 GCM of IPCC (2013) downscaled by WRF, the streamflow of the Mackenzie at the Fort Simpson and Arctic Red River stations. The results show a general decrease of streamflow. Under a warmer future climate, more evaporation loss is expected in the summer which could offset the projected increase in summer precipitation, resulting in an overall decrease in streamflow and lower water levels in 2050s. The projected lower water levels could affect the navigability and the northern ferry operations of the Mackenzie River.

REFERENCES

Agriculture and Agri-Food Canada. 2015. Geospatial Products. Available at: http://www.agr.gc.ca/eng/?id=1343066456961. [Accessed 23 June 2015].

Alexander, L.V., Zhang, X., Peterson, T.C., Caesar, J., Gleason, B., Klein Tank, A.M.G., Haylock, M., Collins, D., Trewin, B., Rahimzadeh, F. and Tagipour, A., 2006. Global observed changes in daily climate extremes of temperature and precipitation. Journal of Geophysical Research: Atmospheres, 111(D5).

Andréasson, J., Bergström, S., Carlsson, B., Graham, L.P. and Lindström, G., 2004. Hydrological change-climate change impact simulations for Sweden. AMBIO: A Journal of the Human Environment, 33(4), pp.228-234.

Arctic Theme Page. 2009. Arctic Council Arctic Marine Shipping Assessment 2009 Report. Available at:http://www.arctic.noaa.gov/detect/documents-/AMSA_2009_Report_2nd_print.pdf. [Accessed 22 July 2015].

Aziz, O.I.A. and Burn, D.H., 2006. Trends and variability in the hydrological regime of the Mackenzie River Basin. Journal of hydrology, 319(1), pp.282-294.

Barrow, E, B. Maxwell and P. Gachon (Eds), 2004. Climate Variability and Change in Canada: Past, Present and Future. ACSD Science Assessment Series No. 2, Meteorological Service of Canada, Environment Canada, Toronto, Ontario, pp. 114.

Benjamin, S.G., Grell, G.A., Brown, J.M., Smirnova, T.G. and Bleck, R., 2004. Mesoscale weather prediction with the RUC hybrid isentropic-terrain-following coordinate model. Monthly Weather Review, 132(2), pp.473-494.

Bergstrom, S., Carlsson, B., Gardelin, M., Lindstrom, G., Pettersson, A. and Rummukainen, M., 2001. Climate change impacts on runoff in Sweden-assessments by global climate models, dynamical downscaling and hydrological modelling. Climate research, 16(2), pp.101-112.

Bowden, J.H., Nolte, C.G. and Otte, T.L., 2013. Simulating the impact of the large-scale circulation on the 2-m temperature and precipitation climatology. Climate dynamics, 40(7-8), pp.1903-1920.

Brimelow, J.C. and Reuter, G.W., 2005. Transport of atmospheric moisture during three extreme rainfall events over the Mackenzie River basin. Journal of Hydrometeorology, 6(4), pp.423-440.

Brimelow, J.C. and Reuter, G.W., 2008. Moisture sources for extreme rainfall events over the Mackenzie River Basin. In Cold Region Atmospheric and Hydrologic Studies. The Mackenzie GEWEX Experience (pp. 127-136). Springer Berlin Heidelberg.

Chou, M.D. and Suarez, M.J., 1999. A solar radiation parameterization for atmospheric studies. NASA Tech. Memo, 104606, p.40.

Chylek, P., Li, J., Dubey, M.K., Wang, M. and Lesins, G., 2011. Observed and model simulated 20th century Arctic temperature variability: Canadian earth system model CanESM2. Atmospheric Chemistry and Physics Discussions, 11(8), pp.22893-22907.

Dasari, H.P., Salgado, R., Perdigao, J. and Challa, V.S., 2014. A Regional Climate Simulation Study Using WRF-ARW Model over Europe and Evaluation for Extreme Temperature Weather Events. International Journal of Atmospheric Sciences, 2014(13). pp.1-22.

Done, J.M., Leung, R.L., Davis, C.A. and Kuo, B, 2004. Regional Climate Simulation using the WRF model. http://www2.mmm.ucar.edu/mm5/workshop/ws04/PosterSession/Done.James.pdf. Presented at the 5th WRF / 14th MM5 Users' Workshop NCAR , June 22-25, 2004.

Dudhia, J., 1989. Numerical study of convection observed during the winter monsoon experiment using a mesoscale two-dimensional model. Journal of the Atmospheric Sciences, 46(20), pp.3077-3107.

Dudhia, J., 1996, July. A multi-layer soil temperature model for MM5. In Preprints, The Sixth PSU/NCAR mesoscale model users' workshop (pp. 22-24).

ECMWF. 2015. *ERA Interim, Daily.* Available at: http://apps.ecmwf.int/datasets/data/interim-full-daily/levtype=sfc/. [Accessed 20 February 2016].

Environment Canada. 2003. Canadian Centre for Climate Modelling and Analysis. Available at: http://www.cccma.ec.gc.ca/data/cgcm4/CanESM2/index.shtml. [Accessed 3 February 2016].

Environment Canada. 2013. HYDAT Database. Available at: https://www.ec.gc.ca/rhc-wsc/default.asp?lang=En&n=9018B5EC-1. [Accessed 13 October 2015].

Fathalli, B., Pohl, B., Castel, T. and Safi, M.J, 2014. Evaluation of a surface temperature simulation over Tunisia using the WRF model. International Lund Regional-Scale Climate Modelling Workshop, 21stCentury Challenges in Regional Climate Modelling Lund, Sweden.

Flesch, T.K. and Reuter, G.W., 2012. WRF model simulation of two Alberta flooding events and the impact of topography. Journal of Hydrometeorology, 13(2), pp.695-708.

Frich, P., Alexander, L.V., Della-Marta, P., Gleason, B., Haylock, M., Klein Tank, A.M. and Peterson, T., 2002. Observed coherent changes in climatic extremes during the second half of the twentieth century. Climate research, 19(3), pp.193-212.

GISTEMP Team. 2015. GISS Surface Temperature Analysis (GISTEMP). NASA Goddard Institute for Space Studies. Dataset accessed 20YY-MM-DD at http://data.giss.nasa.gov/gistemp/.[Accessed 25 October 2015].

Groisman, P.Y., Knight, R.W., Karl, T.R., Easterling, D.R., Sun, B. and Lawrimore, J.H., 2004. Contemporary changes of the hydrological cycle over the contiguous United States: Trends derived from in situ observations. Journal of hydrometeorology, 5(1), pp.64-85.

Gula, J. and Peltier, W.R., 2012. Dynamical downscaling over the Great Lakes basin of North America using the WRF regional climate model: the impact of the Great Lakes system on regional greenhouse warming. Journal of Climate, 25(21), pp.7723-7742.

Hamon, W.R., 1961. Estimating potential evapotranspiration. Journal of the Hydraulics Division, 87(3), pp.107-120.

Held, I.M. and Soden, B.J., 2006. Robust responses of the hydrological cycle to global warming. Journal of Climate, 19(21), pp.5686-5699.

Hong, S.Y., Dudhia, J. and Chen, S.H., 2004. A revised approach to ice microphysical processes for the bulk parameterization of clouds and precipitation. Monthly Weather Review, 132(1), pp.103-120.

Hong, S.Y., Noh, Y. and Dudhia, J., 2006. A new vertical diffusion package with an explicit treatment of entrainment processes. Monthly Weather Review, 134(9), pp.2318-2341.

Iacono, M.J., Delamere, J.S., Mlawer, E.J., Shephard, M.W., Clough, S.A. and Collins, W.D., 2008. Radiative forcing by long-lived greenhouse gases: Calculations with the AER radiative transfer models. Journal of Geophysical Research: Atmospheres, 113(D13).

IPCC, 2013. Climate Change 2013: The Physical Science Basis. Contribution of Working Group I to the Fifth Assessment Report of the Intergovernmental Panel on Climate Change [Stocker, T.F., D. Qin, G.-K. Plattner, M. Tignor, S.K. Allen, J. Boschung, A. Nauels, Y. Xia, V. Bex and P.M. Midgley (eds.)]. Cambridge University Press, Cambridge, United Kingdom and New York, NY, USA, doi:10.1017/CBO9781107415324.

Jin, J., Miller, N.L. and Schlegel, N., 2010. Sensitivity study of four land surface schemes in the WRF model. Advances in Meteorology, 2010.

Kiktev, D., Sexton, D.M., Alexander, L. and Folland, C.K., 2003. Comparison of modeled and observed trends in indices of daily climate extremes. Journal of Climate, 16(22), pp.3560-3571.

Kunkel, K.E., Andsager, K. and Easterling, D.R., 1999. Long-term trends in extreme precipitation events over the conterminous United States and Canada. Journal of climate, 12(8), pp.2515-2527.

Livneh, B., Xia, Y., Mitchell, K.E., Ek, M.B. and Lettenmaier, D.P., 2010. Noah LSM snow model diagnostics and enhancements. Journal of Hydrometeorology, 11(3), pp.721-738.

Maussion, F., D. Scherer, R. Finkelnburg, J. Richters, W. Yang, and T. Yao, 2011. WRF simulation of a precipitation event over the Tibetan Plateau, China—An assessment using remote sensing and ground observations. Hydrology Earth System Science, **15**, pp.1795–1817.

Mekis, É. and Vincent, L.A., 2011. An overview of the second generation adjusted daily precipitation dataset for trend analysis in Canada. Atmosphere-Ocean, 49(2), pp.163-177.

Mölders, N. and Kramm, G., 2010. A case study on wintertime inversions in Interior Alaska with WRF. Atmospheric Research, 95(2), pp.314-332.

Mooney, P.A., Mulligan, F.J. and Fealy, R., 2013. Evaluation of the sensitivity of the weather research and forecasting model to parameterization schemes for regional climates of Europe over the period 1990–95. Journal of Climate, 26(3), pp.1002-1017.

Nash, J.E. and Sutcliffe, J.V., 1970. River flow forecasting through conceptual models part I—A discussion of principles. Journal of hydrology, 10(3), pp.282-290.

Natural Resources Canada. 2016. Climate Change Data. Available at: http://www.nrcan.gc.ca/environment/resources/data/11017. [Accessed 7 January 2016].

Newton, B.W., Prowse, T.D. and Bonsal, B.R., 2014. Evaluating the distribution of water resources in western Canada using synoptic climatology and selected teleconnections. Part 2: summer season. Hydrological Processes, 28(14), pp.4235-4249.

NOAA Earth System Research Laboratory. 2015. ESRL Theme Team Presentation. Available at: http://www.esrl.noaa.gov/research/themes/pbl/LandSurfaceProcesses.pdf. [Accessed 20 February 2016].

Oki, T. and Kanae, S., 2006. Global hydrological cycles and world water resources. science, 313(5790), pp.1068-1072.

Pei, L., Moore, N., Zhong, S., Luo, L., Hyndman, D.W., Heilman, W.E. and Gao, Z., 2014. WRF model sensitivity to land surface model and cumulus parameterization under short-term climate extremes over the southern great plains of the United States. Journal of Climate, 27(20), pp.7703-7724.

Pennelly, C., Reuter, G. and Flesch, T., 2014. Verification of the WRF model for simulating heavy precipitation in Alberta. Atmospheric Research, 135, pp.172-192.

Pérez, J.C., Díaz, J.P., González, A., Expósito, J., Rivera-López, F. and Taima, D., 2014. Evaluation of WRF parameterizations for dynamical downscaling in the Canary Islands. Journal of Climate, 27(14), pp.5611-5631.

Pidwirny, M., 2006. The greenhouse effect. Fundamentals of Physical Geography, 2nd Edition. http://www. physicalgeography. net/fundamentals.

Prabha, T.V., Hoogenboom, G. and Smirnova, T.G., 2011. Role of land surface parameterizations on modeling cold-pooling events and low-level jets. Atmospheric Research, 99(1), pp.147-161.

Prolog Canada. 2011. Assessing Emission Reductions from Potential Climate Policies in the Northwest Territories. Available at: http://www.prologcanada.com/projects/. [Accessed 8 December 2015].

Pryor, S.C., Barthelmie, R.J., Young, D.T., Takle, E.S., Arritt, R.W., Flory, D., Gutowski, W.J., Nunes, A. and Roads, J., 2009. Wind speed trends over the contiguous United States. Journal of Geophysical Research: Atmospheres, 114(D14).

Qian, B., Gameda, S., de Jong, R., Falloon, P. and Gornall, J., 2010. Comparing scenarios of Canadian daily climate extremes derived using a weather generator. Climate research (Open Access for articles 4 years old and older), 41(2), p.131.

Research Application Laboratory. 2015. Assessing Emission Land-Surface Atmosphere Interactions: Technology. Available at: http://www.ral.ucar.edu/research/land/technology/-lsm.php. [Accessed 8 December 2015].

Shabbar, A., Bonsal, B. and Khandekar, M., 1997. Canadian precipitation patterns associated with the Southern Oscillation. Journal of Climate, 10(12), pp.3016-3027.

Smirnova, T.G., Benjamin, S.G., Brown, J.M. and Kim, D., 2004. Cycled Snow State in RUC Coupled Data Assimilation System (CDAS). Available at: http://ruc.noaa.gov/pdf/AMS-Sea-2004/CDASpaper_smirnova.pdf. [Accessed 8 December 2015].

Statistics Canada. 2015. Temperature trends in Canada. Available at: http://www.statcan.gc.ca/pub/16-002-x/2011001/ct018-eng.htm. [Accessed 8 December 2015].

Stewart, I.T., Cayan, D.R. and Dettinger, M.D., 2004. Changes in snowmelt runoff timing in western North America under abusiness as usual'climate change scenario. Climatic Change, 62(1-3), pp.217-232.

Szeto, K.K., Tran, H., MacKay, M.D., Crawford, R. and Stewart, R.E., 2008a. The MAGS water and energy budget study. Journal of Hydrometeorology, 9(1), pp.96-115.

Szeto, K.K., Liu, J. and Wong, A., 2008b. Precipitation recycling in the Mackenzie and three other major river basins. In Cold region atmospheric and hydrologic studies. The Mackenzie GEWEX experience (pp. 137-154). Springer Berlin Heidelberg.

Taylor, K.E., 2001. Summarizing multiple aspects of model performance in a single diagram. Journal of Geophysical Research: Atmospheres, 106(D7), pp.7183-7192.

Tewari, M., Guenther, A. and Wiedinmyer, C., 2009. Impacts of weather conditions modified by urban expansion on surface ozone: comparison between the Pearl River Delta and Yangtze River Delta regions. Advances in Atmospheric Sciences, 26(5), pp.962-972.

Trenberth, K.E., Dai, A., Rasmussen, R.M. and Parsons, D.B., 2003. The changing character of precipitation. Bulletin of the American Meteorological Society, 84(9), pp.1205-1217.

Trenberth, K.E., Smith, L., Qian, T., Dai, A. and Fasullo, J., 2007. Estimates of the global water budget and its annual cycle using observational and model data. Journal of Hydrometeorology, 8(4), pp.758-769.

Vehviläinen, B. and Huttunen, M., 1997. Climate change and water resources in Finland. Boreal Environment Research, 2(1), pp.3-18.

Vincent, L.A. and Mekis, E., 2006. Changes in daily and extreme temperature and precipitation indices for Canada over the twentieth century. Atmosphere-Ocean, 44(2), pp.177-193.

Vincent, L.A., Wang, X.L., Milewska, E.J., Wan, H., Yang, F. and Swail, V., 2012. A second generation of homogenized Canadian monthly surface air temperature for climate trend analysis. Journal of Geophysical Research: Atmospheres, 117(D18).

Vincent, L.A., Zhang, X., Brown, R.D., Feng, Y., Mekis, E., Milewska, E.J., Wan, H. and Wang, X.L., 2015. Observed trends in Canada's climate and influence of low-frequency variability modes. Journal of Climate, 28(11), pp.4545-4560.

Water office Canada. 2015. Real-Time Hydrometric Data. Available at: http://wateroffice.ec.gc.ca/mainmenu/real_time_data_index_e.html. [Accessed 8 December 2015].

Wayland, M., 2004. Mackenzie River Basin: State of the Aquatic Ecosystem Report, 2003. [Fort Smith, NWT]: Mackenzie River Basin Board.

Woo, M.K., Rouse, W.R., Stewart, R.E. and Stone, J.M., 2008. The Mackenzie GEWEX Study: a contribution to cold region atmospheric and hydrologic sciences. In Cold Region Atmospheric and Hydrologic Studies. The Mackenzie GEWEX Experience (pp. 1-22). Springer Berlin Heidelberg.

WRF Model Organization. 2015. The Weather Research & Forecasting Model. [ONLINE] Available at: http://www.wrf-model.org/index.php. [Accessed 4 August 2015].

WRF User Page. 2007. LSM group meeting, 17 April 2007. Available at: https://www.atmos.illinois.edu/~snesbitt/ATMS597R/notes/noahLSM-tutorial.pdf. [Accessed 20 February 2016].

WRF Users Page. 2014. User's Guide for the Advanced Research WRF (ARW) Modeling System Version 3.6. Available at: http://www2.mmm.ucar.edu/wrf/users/docs/user_guide_V3.6-/contents.html. [Accessed 8 December 2015].

Yang, D., Shi, X. and Marsh, P., 2015. Variability and extreme of Mackenzie River daily discharge during 1973–2011. Quaternary International, 380, pp.159-168.

Zhang, C., Wang, Y., Lauer, A. and Hamilton, K., 2012. Configuration and evaluation of the WRF model for the study of Hawaiian regional climate. Monthly Weather Review, 140(10), pp.3259-3277.

Zhang, H., Pu, Z. and Zhang, X., 2013. Examination of errors in near-surface temperature and wind from WRF numerical simulations in regions of complex terrain. Weather and Forecasting, 28(3), pp.893-914.

Zhang, X., Vincent, L.A., Hogg, W.D. and Niitsoo, A., 2000. Temperature and precipitation trends in Canada during the 20th century. Atmosphere-ocean, 38(3), pp.395-429.

APPENDIX A

A.1

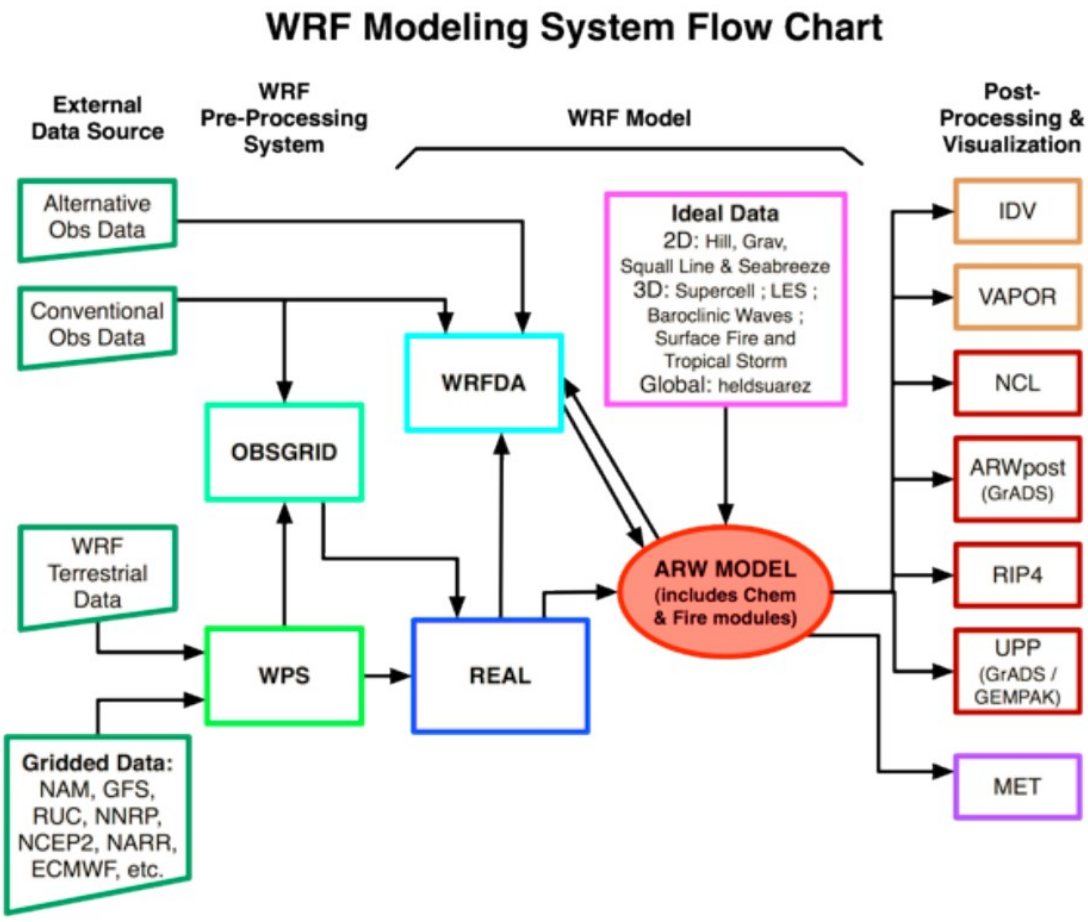

WRF Modeling System (WRF Users Page 2014)

A.2 WRF model physics parameterization used in the experiments

Micro Physics Options *(mp_physics)*		
Kessler Scheme	**option 1**	Kessler, E., 1969: On the distribution and continuity of water substance in atmoshperic circulations. *Meteor. Monogr.*, **32**, Amer. Meteor. Soc.
Lin et al. Scheme	**option 2**	Lin, Yuh–Lang, Richard D. Farley, and Harold D. Orville, 1983: Bulk Parameterization of the Snow Field in a Cloud Model. *J.Climate Appl. Met.*, **22**, 1065–1092.
WRF Single–moment 3–class and 5–class Schemes	**options 3 & 4**	Hong, Song–You, Jimy Dudhia, and Shu–Hua Chen, 2004: A revised approach to ice microphysical processes for the bulk parameterization of clouds and precipitation. *Mon. Wea. Rev.*, **132,** 103–120.
WRF Single–moment 6–class Scheme	**option 6**	Hong, S.–Y., and J.–O. J. Lim, 2006: The WRF single–moment 6–class microphysics scheme (WSM6). *J. Korean Meteor. Soc.*, **42**, 129–151.
WRF Double Moment 5–class and 6–class Schemes	**options 14 & 16**	Lim, K.–S. S., and S.–Y. Hong, 2010: Development of an effective double–moment cloud microphysics scheme with prognostic cloud condensation nuclei (CCN) for weather and climate models. *Mon. Wea. Rev.*, **138**, 1587–1612.

Planetary Boundary Layer (PBL) Physics Options *(bl_pbl_physics)*		
Yonsei University Scheme (YSU)	**option 1**	Hong, Song–You, Yign Noh, Jimy Dudhia, 2006: A new vertical diffusion package with an explicit treatment of entrainment processes. *Mon. Wea. Rev.*, **134**, 2318–2341.
Mellor–Yamada–Janjic Scheme (MYJ)	**option 2**	Janjic, Zavisa I., 1994: The Step–Mountain Eta Coordinate Model: Further developments of the convection, viscous sublayer, and turbulence closure schemes. *Mon. Wea. Rev.*, **122**, 927–945.
TEMF Surface Layer Scheme	**option 10**	Angevine, Wayne M., Hongli Jiang, and Thorsten Mauritsen, 2010: Performance of an eddy diffusivity–mass flux scheme for shallow cumulus boundary layers. *Mon. Wea. Rev.*, **138**, 2895–2912.

Cumulus Parameterization Options *(cu_physics)*		
Kain–Fritsch Scheme	**option 1**	Kain, John S., 2004: The Kain–Fritsch convective parameterization: An update. *J. Appl. Meteor.*, **43**, 170–181.

Betts–Miller–Janjic Scheme	**option 2**	Janjic, Zavisa I., 1994: The Step–Mountain Eta Coordinate Model: Further developments of the convection, viscous sublayer, and turbulence closure schemes. *Mon. Wea. Rev.*, **122**, 927–945.
Tiedtke Scheme	**option 6**	Tiedtke, M., 1989: A comprehensive mass flux scheme for cumulus parameterization in large–scale models. *Mon. Wea. Rev.*, **117**, 1779–1800. Zhang, Chunxi, Yuqing Wang, and Kevin Hamilton, 2011: Improved representation of boundary layer clouds over the southeast pacific in ARW–WRF using a modified Tiedtke cumulus parameterization scheme. *Mon. Wea. Rev.*, **139**, 3489–3513.

Shortwave *(ra_sw_physics)* and Longwave *(ra_lw_physics)* Options		
Dudhia Shortwave Scheme	**option 1**	Dudhia, J., 1989: Numerical study of convection observed during the Winter Monsoon Experiment using a mesoscale two–dimensional model. *J. Atmos. Sci.*, **46**, 3077–3107.
RRTM Longwave Scheme	**option 1**	Mlawer, Eli. J., Steven. J. Taubman, Patrick. D. Brown, M. J. Iacono, and S. A. Clough (1997), Radiative transfer for inhomogeneous atmospheres: RRTM, a validated correlated–k model for the longwave. *J. Geophys. Res.*, **102**,

		16663–16682.
Goddard Shortwave Scheme	**option 2**	Chou, Ming–Dah, and Max J. Suarez, 1994: An efficient thermal infrared radiation parameterization for use in general circulation models. *NASA Tech. Memo,* 84 pp.
CAM Shortwave and Longwave Schemes	**option 3**	Collins, William D., et al., 2004: Description of the NCAR Community Atmosphere Model (CAM 3.0). NCAR Tech. Note NCAR/TN–464+STR. 214 pp.
RRTMG Shortwave and Longwave Schemes	**option 4**	Iacono, M. J., J. S. Delamere, E. J. Mlawer, M. W. Shephard, S. A. Clough, and W. D. Collins, 2008: Radiative forcing by long–lived greenhouse gases: Calculations with the AER radiative transfer models. *J. Geophys. Res.*, **113**, D13103.
New Goddard Shortwave and Longwave Schemes	**option 5**	Chou, Ming–Dah, and Max J. Suarez, 1999: A solar radiation parameterization for atmospheric studies. *NASA Tech. Memo 104606* **40**.
Fu–Liou–Gu Shortwave and Longwave	**option 7**	Gu, Y., Liou, K. N., Ou, S. C., and Fovell, R., 2011: Cirrus cloud simulations using WRF with improved radiation parameterization and increased vertical resolution. *J.*

Schemes		*Geophys. Res.*, **116**, D06119. Fu, Qiang, and K. N. Liou, 1992: On the correlated k–distribution method for radiative transfer in nonhomogeneous atmospheres. *J. Atmos. Sci.*, **49**, 2139–2156.

Land Surface Options *(sf_surface_physics)*		
5–layer Thermal Diffusion Scheme	**option 1**	Dudhia, Jimy, 1996: A multi-layer soil temperature model for MM5. the Sixth PSU/NCAR Mesoscale Model Users' Workshop.
Unified Noah Land Surface Model	**option 2**	Tewari, M., F. Chen, W. Wang, J. Dudhia, M. A. LeMone, K. Mitchell, M. Ek, G. Gayno, J. Wegiel, and R. H. Cuenca, 2004: Implementation and verification of the unified NOAH land surface model in the WRF model. *20th conference on weather analysis and forecasting/16th conference on numerical weather prediction*, pp. 11–15.
RUC Land Surface Model	**option 3**	Benjamin, Stanley G., Georg A. Grell, John M. Brown, and Tatiana G. Smirnova, 2004: Mesoscale weather prediction with the RUC hybrid isentropic-terrain-following coordinate model.

		Mon. Wea. Rev., **132**, 473-494.

Surface Layer Options *(sf_sfclay_physics)*		
MM5 Similarity Scheme	**option 1**	Paulson, C. A., 1970: The mathematical representation of wind speed and temperature profiles in the unstable atmospheric surface layer. *J. Appl. Meteor.*, **9**, 857–861. Dyer, A. J., and B. B. Hicks, 1970: Flux–gradient relationships in the constant flux layer. *Quart. J. Roy. Meteor. Soc.*, **96**, 715–721. Webb, E. K., 1970: Profile relationships: The log-linear range, and extension to strong stability. *Quart. J. Roy. Meteor. Soc.*, **96**, 67–90. Beljaars, A.C.M., 1994: The parameterization of surface fluxes in large-scale models under free convection. *Quart. J. Roy. Meteor. Soc.*, **121**, 255–270. Zhang, D.–L., and R.A. Anthes, 1982: A high–resolution model of the planetary boundary layer– sensitivity tests and comparisons with SESAME–79 data. *J. Appl. Meteor.*, **21**,

		1594–1609.
Eta Similarity Scheme	**option 2**	Monin A. S., and A. M. Obukhov, 1954: Basic laws of turbulent mixing in the surface layer of the atmosphere. Contrib Geophys Inst Acad Sci USSR 151:163–187 (in Russian) Janjic, Z. I., 1994: The step-mountain Eta coordinate model: further developments of the convection, viscous sublayer and turbulence closure schemes. *Mon. Wea. Rev.*, **122**, 927–945. Janjic, Z. I., 1996: The surface layer in the NCEP Eta Model. *Eleventh conference on numerical weather prediction, Norfolk, VA, 19–23 August 1996. Amer Meteor Soc, Boston, MA,* pp 354–355. Janjic, Z. I., 2002: Nonsingular implementation of the Mellor-Yamada Level 2.5 Scheme in the NCEP Meso model. *NCEP Office Note No. 437,* 61 pp.